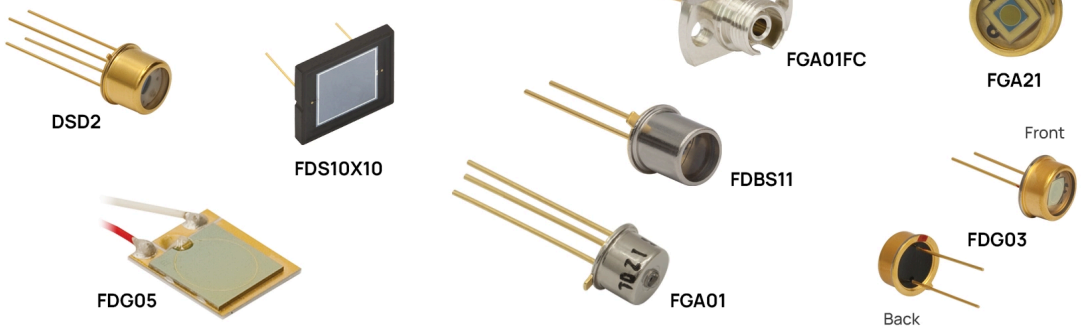
FDG10X10 - August 13, 2026

Item # FDG10X10 was discontinued on August 13, 2026. For informational purposes, this is a copy of the website content at that time and is valid only for the stated product.

LIGHT ANALYSIS

Photodiodes

- Si, Black Si, Dual Band (Si/InGaAs), Ge, and InGaAs Detectors Available
- Available in TO Can, FC Connector, and Flat Wafer Body Styles
- Available in Hermetically Sealed Packages



Related Items

Amplified Photodetectors



MIR Photodiodes



Thermopile Power Detectors



Transimpedance Amplifiers



Overview

Features

- Si, Black Si, Dual Band (Si/InGaAs), Ge, and InGaAs Unmounted Photodiodes Available
- Wavelength Ranges from 200 to 2600 nm
- FDS100 Si Photodiode Also Available in Packs of 5, 10, or 50

Mounted and Unmounted Detectors
Photodiodes
Mounted Photodiodes (200 - 2600 nm)
Unmounted Photodiodes (200 - 2600 nm)
Pigtailed Photodiodes (320 - 1000 nm)
Calibrated Photodiodes (350 - 1800 nm)
Photovoltaic Detectors (2000 - 10 600 nm)
Thermopile Detectors (190 - 20 000 nm)
Pyroelectric Detector (600 - 16 000 nm)

Thorlabs stocks a wide selection of photodiodes (PD) with various active area sizes and packages. Discrete PIN junction photodiodes include silicon (Si), black silicon (B-Si), and indium gallium arsenide (InGaAs) materials. Germanium (Ge) photodiodes, which are based on an N-on-P structure, are also available.

Our fastest photodiodes are the FDS015, FDS02, and FDS025 Si photodiodes. The FDS015 Si photodiode has a 35 ps rise time and a 0.65 pF junction capacitance, making it the highest speed, lowest capacitance photodiode offered below. Alternatively, the FD11A Si photodiode has a dark current of 2 pA, making it our photodiode with the lowest dark current. We also offer the FDBS11, FDBS22, and FDBS25 black Si photodiodes, which feature a higher responsivity across the 240 to 1170 nm wavelength range than standard Si photodiodes. The DSD2 is a dual-band photodiode, which incorporates two photodetectors sandwiched on top of each other (Si substrate on top of an InGaAs substrate), offering a combined wavelength range of 400 to 1800 nm. The FD05D and FD10D are InGaAs photodiodes with high responsivity from 900 to 2600 nm, allowing detection of wavelengths beyond the normal 1800 nm range of typical InGaAs photodiodes.

To complement our photodiode product line, we offer mounted photodiodes and a range of compatible photodiode sockets. Please note that the PDs sold below are not calibrated, meaning responsivity will differ slightly from lot to lot; refer to the *Response Variation* tab for more information. We also offer calibrated photodiodes, which come with NIST-traceable calibration, to correct for the differences in responsivity. Many of our photodiodes can be reverse voltage biased using the PBM42 DC Bias Module for faster speed and higher optical power detection.

For information on the photodiode saturation limit and the noise floor, as well as a collection of Thorlabs-conducted experiments regarding spatial uniformity (or varying responsivity) and dark current as a function of temperature, refer to the *Lab Facts* tab. This tab also outlines the theory and methods we use to define the specifications of our photodiodes. For example, the Noise Equivalent Power (NEP) as a Function of Temperature section provides background on NEP values specified by shot noise and thermal noise. With zero bias (Photovoltaic Mode), the NEP is specified by the thermal noise only, which is caused by the shunt resistance of the photodiode. The *Photodiode Tutorial* provides more general information regarding the operation, terminology, and theory of photodiodes.

Inhomogeneity on the edge of an active area of the detector can generate unwanted capacitance and resistance that distorts the time-domain response of a photodiode. Thorlabs therefore recommends that the incident light on the photodiode is well centered on the active area. This can be accomplished by placing a focusing lens or pinhole in front of the detector element.

Thorlabs offers spectral-flattening filters that are designed to improve the response uniformity of our silicon photodiodes. Click here to learn more.

Response Variation

The responsivity of a particular photodiode varies from lot to lot. Due to this, the photodiode you receive may have a slightly different response than what is represented below. For example, in Figure 2.1, a graph for the FDS1010 photodiode shows the extent that the response may vary. This data was collected from 104 photodiodes. Minimum, Average, and Maximum responsivity was calculated at each data point and has been plotted.

To view typical responsivity vs. wavelength data for each individual photodiode, please click the info icons (ⓘ) in Tables G1.1 through G5.1.

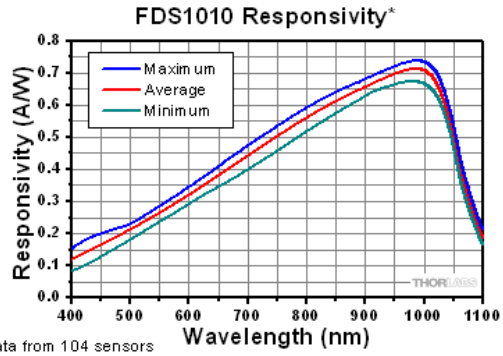


Figure 2.1 FDS1010 Photodiode Response Varies from Lot to Lot

Photodiode Tutorial

Theory of Operation

A junction photodiode is an intrinsic device that behaves similarly to an ordinary signal diode, but it generates a photocurrent when light is absorbed in the depleted region of the junction semiconductor. A photodiode is a fast, highly linear device that exhibits high quantum efficiency and may be used in a variety of different applications.

It is necessary to be able to correctly determine the level of the output current to expect and the responsivity based upon the incident light. Depicted in Figure 100A is a junction photodiode model with basic discrete components to help visualize the main characteristics and gain a better understanding of the operation of Thorlabs' photodiodes.

$$I_{OUT} = I_{DARK} + I_{PD}$$

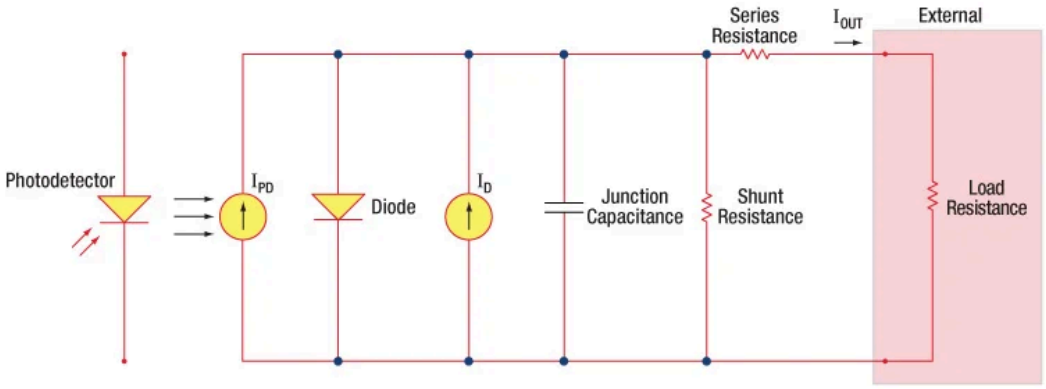


Figure 100A Photodiode Model

Photodiode Terminology

Responsivity

The responsivity of a photodiode can be defined as a ratio of generated photocurrent (I_{PD}) to the incident light power (P) at a given wavelength:

$$R(\lambda) = \frac{I_{PD}}{P}$$

Modes of Operation (Photoconductive vs. Photovoltaic)

A photodiode can be operated in one of two modes: photoconductive (reverse bias) or photovoltaic (zero-bias). Mode selection depends upon the application's speed requirements and the amount of tolerable dark current (leakage current).

Photoconductive

In photoconductive mode, an external reverse bias is applied, which is the basis for our DET series detectors. The current measured through the circuit indicates illumination of the device; the measured output current is linearly proportional to the input optical power. Applying a reverse bias increases the width of the depletion junction producing an increased responsivity with a decrease in junction capacitance and produces a very linear response. Operating under these conditions does tend to produce a larger dark current, but this can be limited based upon the photodiode material. (Note: Our DET detectors are reverse biased and cannot be operated under a forward bias.)

Photovoltaic

In photovoltaic mode the photodiode is zero biased. The flow of current out of the device is restricted and a voltage builds up. This mode of operation exploits the photovoltaic effect, which is the basis for solar cells. The amount of dark current is kept at a minimum when operating in photovoltaic mode.

Dark Current

Dark current is leakage current that flows when a bias voltage is applied to a photodiode. When operating in a photoconductive mode, there tends to be a higher dark current that varies directly with temperature. Dark current approximately doubles for every 10 °C increase in temperature, and shunt resistance tends to double for every 6 °C rise. Of course, applying a higher bias will decrease the junction capacitance but will increase the amount of dark current present.

The dark current present is also affected by the photodiode material and the size of the active area. Silicon devices generally produce low dark current compared to germanium devices which have high dark currents. Table 100B lists several photodiode materials and their relative dark currents, speeds, spectral ranges, and costs.

Table 100B Photodiode Materials				
Material	Dark Current	Speed	Spectral Range	Cost
Silicon (Si)	Low	High Speed	Visible to NIR	Low
Black Silicon (B-Si)	Low	Medium Speed[a]	Visible to NIR	Moderate
Germanium (Ge)	High	Low Speed	NIR	Low
Indium Gallium Arsenide (InGaAs)	Low	High Speed	NIR	Moderate
Indium Arsenide Antimonide (InAsSb)	High	Low Speed	NIR to MIR	High
Extended Range Indium Gallium Arsenide (InGaAs)	High	High Speed	NIR	High
Mercury Cadmium Telluride (MCT, HgCdTe)	High	Low Speed	NIR to MIR	High

a. While B-Si photodiodes are typically slower than Si, they feature higher responsivities across the wavelength range.

Junction Capacitance

Junction capacitance (C_j) is an important property of a photodiode as this can have a profound impact on the photodiode's bandwidth and response. It should be noted that larger diode areas encompass a greater junction volume with increased charge capacity. In a reverse bias application, the depletion width of the junction is increased, thus effectively reducing the junction capacitance and increasing the response speed.

Bandwidth and Response

A load resistor will react with the photodetector junction capacitance to limit the bandwidth. For best frequency response, a 50 Ω terminator should be used in conjunction with a 50 Ω coaxial cable. The bandwidth (f_{BW}) and the rise time response (t_r) can be approximated using the junction capacitance (C_j) and the load resistance (R_{LOAD}):

$$f_{BW} = 1 / (2 * \pi * R_{LOAD} * C_j)$$
$$t_r = 0.35 / f_{BW}$$

Noise Equivalent Power

The noise equivalent power (NEP) is the input signal power that results in a signal-to-noise ratio (SNR) of 1 in a 1 Hz output bandwidth. This is useful, as the NEP determines the ability of the detector to detect low level light. In general, the NEP increases with the active area of the detector and is given by the following equation:

$$NEP = \frac{Incident\ Energy * Area}{\frac{S}{N} * \sqrt{\Delta f}}$$

Here, S/N is the Signal to Noise Ratio, Δf is the Noise Bandwidth, and Incident Energy has units of W/cm^2. For more information on NEP, please see Thorlabs' Noise Equivalent Power White Paper.

Terminating Resistance

A load resistance is used to convert the generated photocurrent into a voltage (V_{OUT}) for viewing on an oscilloscope:

$$V_{OUT} = I_{OUT} * R_{LOAD}$$

Depending on the type of the photodiode, load resistance can affect the response speed. For maximum bandwidth, we recommend using a 50 Ω coaxial cable with a 50 Ω terminating resistor at the opposite end of the cable. This will minimize ringing by matching the cable with its characteristic impedance. If bandwidth is not important, you may increase the amount of voltage for a given light level by increasing R_{LOAD}. In an unmatched termination, the length of the coaxial cable can have a profound impact on the response, so it is recommended to keep the cable as short as possible.

Shunt Resistance

Shunt resistance represents the resistance of the zero-biased photodiode junction. An ideal photodiode will have an infinite shunt resistance, but actual values may range from the order of ten Ω to thousands of MΩ and is dependent on the photodiode material. For example, and InGaAs detector has a shunt resistance on the order of 10 MΩ while a Ge detector is in the kΩ range. This can significantly impact the noise current on the photodiode. For most applications, however, the high resistance produces little effect and can be ignored.

Series Resistance

Series resistance is the resistance of the semiconductor material, and this low resistance can generally be ignored. The series resistance arises from the contacts and the wire bonds of the photodiode and is used to mainly determine the linearity of the photodiode under zero bias conditions.

Common Operating Circuits

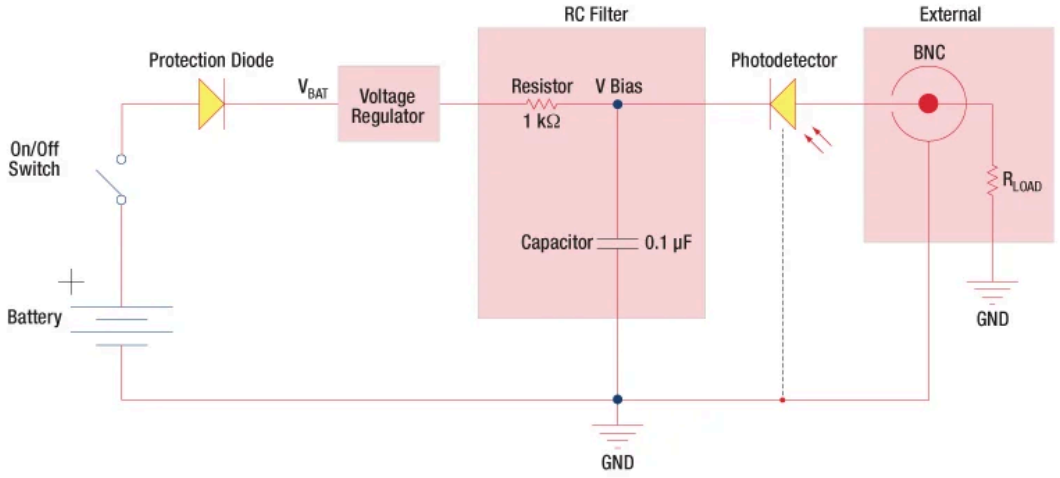


Figure 100C Reverse-Biased Circuit (DET Series Detectors)

The DET series detectors are modeled with the circuit depicted in Figure 100C. The detector is reverse biased to produce a linear response to the applied input light. The amount of photocurrent generated is based upon the incident light and wavelength and can be viewed on an oscilloscope by attaching a load resistance on the output. The function of the RC filter is to filter any high-frequency noise from the input supply that may contribute to a noisy output.

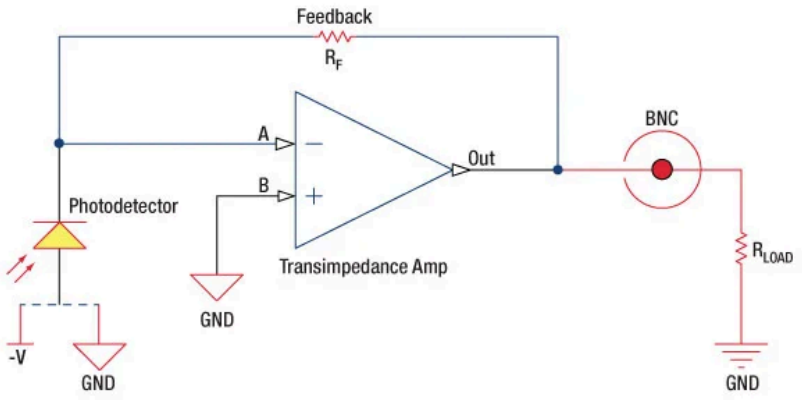


Figure 100D Amplified Detector Circuit

One can also use a photodetector with an amplifier for the purpose of achieving high gain. The user can choose whether to operate in Photovoltaic of Photoconductive modes. There are a few benefits of choosing this active circuit:

- Photovoltaic mode: The circuit is held at zero volts across the photodiode, since point A is held at the same potential as point B by the operational amplifier. This eliminates the possibility of dark current.
- Photoconductive mode: The photodiode is reversed biased, thus improving the bandwidth while lowering the junction capacitance. The gain of the detector is dependent on the feedback element (R_f). The bandwidth of the detector can be calculated using the following:

$$f(-3dB) = \sqrt{\frac{GBP}{4\pi * R_f * C_D}}$$

where GBP is the amplifier gain bandwidth product and C_D is the sum of the junction capacitance and amplifier capacitance.

Effects of Chopping Frequency

The photoconductor signal will remain constant up to the time constant response limit. Many detectors, including PbS, PbSe, HgCdTe (MCT), and InAsSb, have a typical 1/f noise spectrum (i.e., the noise decreases as chopping frequency increases), which has a profound impact on the time constant at lower frequencies.

The detector will exhibit lower responsivity at lower chopping frequencies. Frequency response and detectivity are maximized for

$$f_c = \frac{1}{2\pi\tau_r}$$

Lab Facts

Summary

This tab contains a collection of experiments performed at Thorlabs regarding the performance of photodiodes we offer. Each section is its own independent experiment, which can be viewed by clicking in the appropriate box below. *Photodiode Saturation Limit and Noise Floor* explores how different conditions, including temperature, resistivity, reverse-bias voltage, responsivity, and system bandwidth, can affect noise in a photodiode's output. *Photodiode Spatial Uniformity* explores variations in the responsivity as a small-diameter light beam is scanned across the active area of the photodiode. Photodiodes with different material compositions are tested, and eight units of one silicon-based model are tested to investigate unit-to-unit variations. *Dark Current as a Function of Temperature* and *Noise Equivalent Power (NEP) as a Function of Temperature* describe how dark current and NEP, respectively, vary with temperature and how measurements are affected. *Beam Size and Photodiode Saturation* shows how the photodiode saturation point changes with the incident beam size and investigates several models to explain the results. *Bias Voltage* examines the effects of incident power on the effective reverse bias voltage of a photodiode circuit and verifies a reliable model for predicting those changes.

Photodiode Saturation Limit and Noise Floor

We present laboratory measurements of the saturation limit and noise floor of a Thorlabs silicon photodiode. While all photodiodes function similarly, there are a number of parameters that affect the noise floor and saturation limit of a photodiode including the sensor temperature, resistivity, reverse bias voltage, responsivity, and system bandwidth. Here we investigated the effect of reverse bias voltage and load resistance within a silicon-based photodiode detection system. Increasing the reverse bias increased the saturation limit and had minimal effect on the noise floor. Decreasing the load resistance decreased the noise floor until reaching the noise of the measurement system, but also decreased the saturation limit. These results demonstrate some of the considerations necessary for choosing the reverse bias voltage and load resistance, and emphasize that noise sources within all of the components must be considered when creating a detection system.

For our experiment we used the FDS100 Si Photodiode as the photodiode under investigation. The collimated output of a fiber-pigtailed laser diode was used as the light source with output power from 0 to 50 mW. The collimated beam was incident upon a beamsplitter that transmitted the majority of the light to the photodiode under investigation and reflected the rest towards a reference power sensor. The photodiode response was then evaluated under various resistive loads and with different reverse bias voltages.

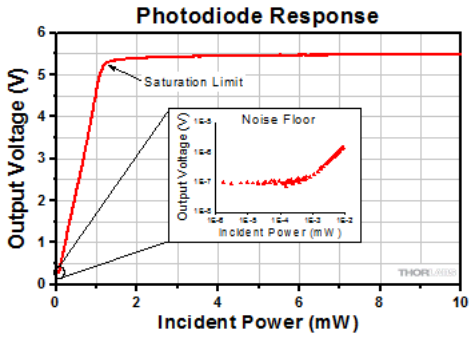


Figure 171A Overview of the Photodiode's Response Curve,
Highlighting the Saturation Limit and the Noise Floor

Lab Facts

Click for Full Lab Facts Summary

Figures 171A through 171D summarize the measured results for the various tested configurations. From these graphs the changes to the photodiode's linear response, noise floor, and saturation limit can be observed under different reverse voltage biases and load resistances. Figure 171A provides an overview of the photodiode response with a reverse voltage bias of 5 V and resistive load of 10 kΩ. The photodiode saturated at the upper limit of the response when the output photovoltage approached the reverse bias voltage. The noise floor at the lower limit of the response was a result of dark current and the thermal noise from the resistive load (Johnson noise). Figure 171B summarizes the results obtained using the photodiode with a 1 kΩ resistive load and various reverse bias voltages. It illustrates that the saturation limit can be raised by increasing the reverse bias voltage (within specification). Figure 171C summarizes the results from using the photodiode with a 5 V reverse bias voltage and various resistive loads. It illustrates that the slope of the photovoltage response increased as the load resistance was increased. Figure 171D summarizes the noise floor results obtained using a 0 V reverse bias voltage and various resistive loads. The noise floor increased when larger load resistances were used. It is important to note that the 1 kΩ data was measured above the theoretical Johnson noise due to the voltage noise within the measurement system. Minimal change in the overall noise floor was seen when using a 5 V reverse bias voltage. For details on the experimental setup employed and these summarized results, please click here.

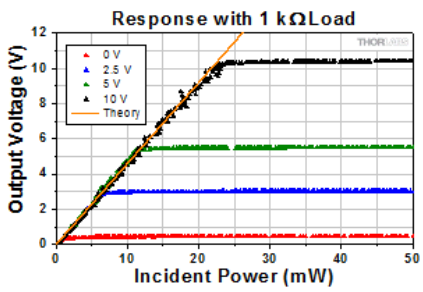


Figure 171B Photovoltage Dependence on Reverse Bias Voltage

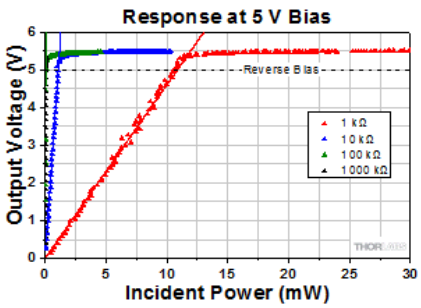


Figure 171C Response with Various Resistive Loads

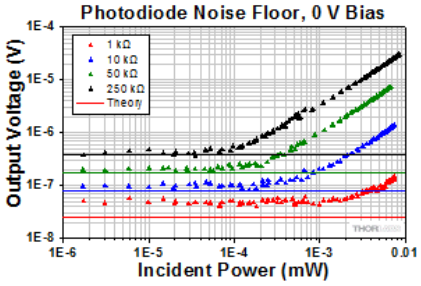


Figure 171D Noise Floor with Various Resistive Loads

Photodiode Spatial Uniformity

Do all regions of a photodiode's active area have the same responsivity?

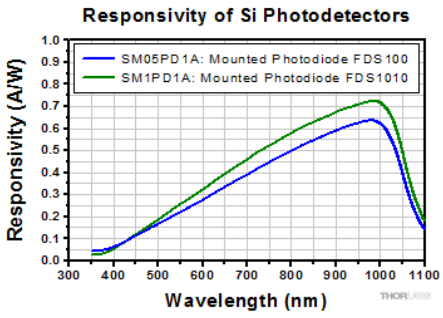


Figure 171E Responsivity, which describes the relationship between the strength of the photocurrent output by the photodetector and the optical power in the incident beam, is dependent on the wavelength of the incident light.

The output signal strength from a photodetector is significantly affected by the optical power and wavelength of the incident light. A measure of this relationship is responsivity, which is the magnitude of the output photocurrent divided by the optical power of the incident light. While responsivity has units of ampere per watt, it also varies with wavelength. Often overlooked is that responsivity can also vary as different regions of the photodiode's active area are illuminated.

This work investigated the change in photodetector response as a light beam, with a diameter that was small in comparison to the active area of the photodiode, was scanned across the active area. A selection photodetectors, based on mounted gallium phosphide (GaP), silicon (Si), indium gallium arsenide (InGaAs), or germanium (Ge) photodiodes, were tested.

Responsivity is Wavelength Dependent[1,2]

One reason responsivity varies with respect to wavelength is the relationship among optical power, wavelength, and photo-generated electrons. A light beam illuminating a surface provides an optical power equal to the energy in the beam divided by the time the surface was illuminated. The energy in a single-wavelength beam equals the number of incident photons times the energy of a single photon. Decreasing the wavelength of the light increases the energy of the photons. If the wavelength is decreased, but the optical power is kept the same, there are fewer incident photons.

A single photon can generate no more than a single electron of photocurrent in these photodetectors. Due to this, reducing the wavelength of the incident light while holding its optical power constant results in a reduced photocurrent. Since responsivity relates the output photocurrent to the incident optical power, instead of to the number of incident photons per unit time, responsivity is lower at lower wavelengths. The responsivity curves plotted in Figure 171E are examples showing responsivity increasing with wavelength.

The upper wavelength of a photodetector's responsivity is limited by inherent properties of the semiconductor material. In order for an incident photon to contribute to the photocurrent, the photon must have enough energy to free an electron from its bonds to its host atom. Photons with wavelengths above the upper wavelength limit do not have enough energy. The semiconductor material composing the photodiode determines the wavelength of this limit.

Response May Vary as Different Regions of the Photodiode's Active Area are Illuminated[1,2]

An electron that has escaped the bonds of its host atom by absorbing the energy of a photon is a photo-generated electron. A photo-generated electron contributes to the photocurrent only if the electron is able to successfully travel from where it was generated, across the semiconductor material, and to an electrical contact. A photo-generated electron does not contribute to the photocurrent if it is re-absorbed by the semiconductor material before reaching a contact, which is a more likely outcome if the electron encounters a defect.

Defects are places where the semiconductor's crystal lattice is not perfect. These locations include dislocations, impurities, and voids in the crystal lattice. The external surfaces of a real crystal with finite dimensions are also imperfections, since a perfect crystal is infinite in length, height, and width. Defects in the semiconductor crystal absorb photo-generated electrons at a high rate and turn their kinetic energy into heat, rather than allow the electrons to contribute to the photocurrent.

Electrons generated near defects are more likely to be re-absorbed and less likely to contribute to the photocurrent. While the density of defects in a semiconductor can be minimized, the semiconductor crystals used in photodiodes are not perfect. It is also not unusual for the density of defects to vary throughout the volume of the semiconductor crystal, as well as for the growth of some semiconductor materials to be more prone to forming defects than others.

If the density of defects varies throughout the volume of the semiconductor material, the magnitude of the photocurrent generated within each region would be expected to be different. Since the photodetector's responsivity depends on the magnitude of photocurrent, a varying density of defects would result in the responsivity changing as different locations on the photodetector are illuminated. This effect was investigated using the procedure described in the following section.

Experimental Setup and Results

Measurement Objectives

Several photodetectors were tested to investigate the uniformity of the responsivity across their active areas. The spatially dependent responsivities of one GaP-based, four Si-based, two InGaAs-based, and two Ge-based photodetectors were measured at selected wavelengths. Testing was conducted to investigate the spatial uniformity of the responsivity of:

- All nine photodetector models at a wavelength close to the wavelength of peak responsivity. (Results contained in Table 171G.)
- A Si-based, an InGaAs-based, and a Ge-based photodetector at three different wavelengths. (Results contained in Table 171H.)
- Eight different units of a single Si-based photodetector model at a wavelength close to the wavelength of peak responsivity. (Results contained in Table 171J.)

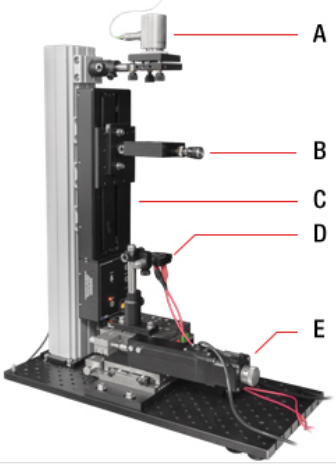


Figure 171F The setup used to measure the change in response across the active area of each photodiode included: a reflective collimator (A), an achromatic doublet lens (B) , vertically-mounted linear translation stage (C), the photodetector under test (D), and two horizontally-mounted translation stages (E) of which one is visible.

Experimental Setup (Components Labeled in Figure 171F Are Labeled in the Following)

The experimental setup consisted of a light source (not shown) that was fiber-coupled to an RC12APC-P01 collimator (A), which was installed in a KM100T kinematic mount. An AC254-150-A achromatic doublet lens with a 150 mm focal length (B), which was installed in a ST1XY-D mount, focused the light on the active area of the photodetector (D), which was mounted with the help of a KB1P magnetic quick-release carriage set. Other components in the vertical arm included a previous-generation LTS150 motorized linear translation stage (C), an XT66P1 vertical mounting plate, an XT66-500 66 mm construction rail, and four XT66C4 clamping platforms. The components in the horizontal arm included two previous-generation LNR50S motorized linear translation stages (E), an LNR50P3 XY adapter plate, a baseplate, and two BSC201 closed-loop stepper motor controllers (not shown), which scanned the beam across the active area of the photodetector (D). Most light sources were products from our Superluminescent Diode series. The exception was the 405 nm light source, which was an S3FC405 benchtop laser source.

Procedure

The diameter of the beam was scaled according to the active area of the photodetector, so that approximately 3600 measurements were taken in a 60 x 60 grid across the surface of each photodiode. The beam diameter used for each photodiode was between 50 µm and 500 µm, and the size used to make a particular measurement is included in the notes that accompany each plot in Tables 171G, 171H, and 171J. To view this information, click on the plot of interest.

During the scan, the position of the beam remained stationary, and the two LNR50S motorized stages were used to translate the photodetector in the two directions perpendicular to the optic axis. To ensure that the entire active area of the photodetector was tested, the dimensions of the scan area exceeded the dimensions of the active area.

No reverse bias voltage was applied to any of the photodiodes during this investigation.

Results (Click Below to Expand Tables 171G, 171H, and 171J)

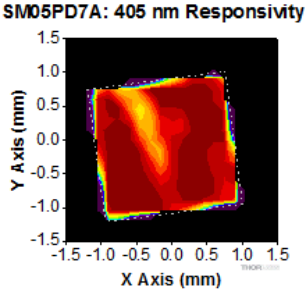
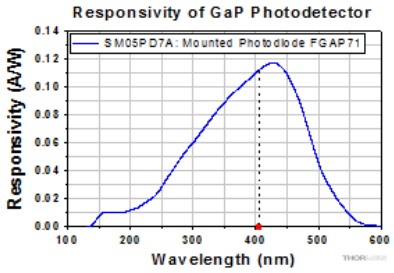
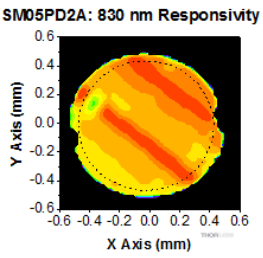
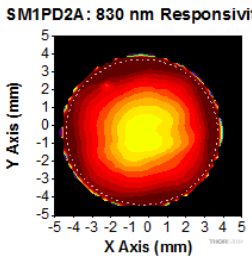
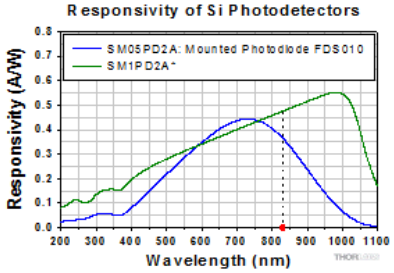
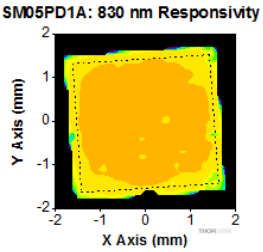
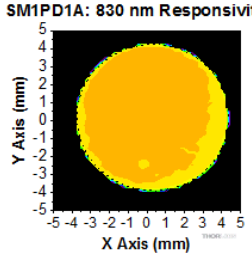
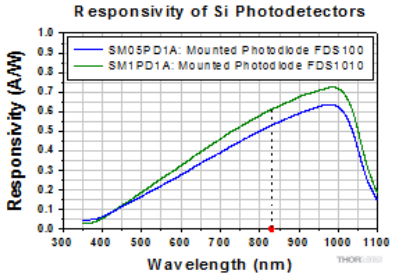
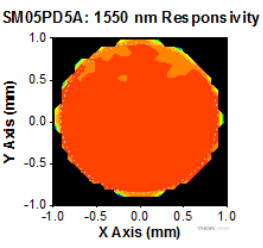
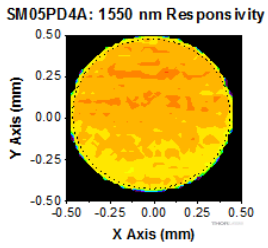
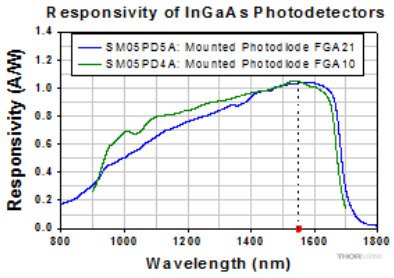
The measurement data were normalized and then plotted with respect to the measurement position. The data in each measurement set were normalized with respect to the value at the center of the active area, which resulted in plots that show the variation of the responsivity across each photodetector's active area and allow the results from these nine different photodetector models to be compared. The plotted data were also processed to remove data points with values indistinguishable from noise. This was done to eliminate data points corresponding to measurements made outside of the active area of each photodetector. However, this approach also removed some measurements made within, but close to, the outer edges of the active areas. The lower photocurrent generated by these regions may have been due to the beam spot partially illuminating regions outside of the active area, as well as photocurrent suppressed by a higher density of defects near the edges.

The plots can be revealed by expanding Tables 171G, 171H, and 171J. Each plot includes a dashed outline surrounding the central 90% of the active area of the photodiode. Under general use, the light beam should remain within this central 90% region to avoid edge effects. Click on each plot to reveal information about the active area of the photodiode and the size of the beam scanned across the active area.

Since these photodetectors represent a small sample size, these measurements are representative of the other photodetectors of its model, but results obtained using other units of the same model may vary. The measurements acquired for these photodetector units were repeatable, but no two semiconductor crystals are identical and unit-to-unit variations should be expected. The following tables show that:

- **Table 171G**: The variations of the responsivities across the active areas of the Ge-based and GaP-based photodetectors are greater than the variations of the responsivities across the active areas of the Si-based and InGaAs-based photodetectors. This suggests the defect densities of the Si-based and InGaAs-based semiconductor materials are more uniform than the defect densities of the Ge-based and GaP-based semiconductor materials.
- **Table 171H**: The variations of the responsivities across the active areas of a Si-based, an InGaAs-based, and a Ge-based photodetector change with wavelength. For each photodetector, the minimum spatial variations of the responsivity occurred when the wavelength of light was near the wavelength of the peak value of responsivity.
- **Table 171J**: Eight units of a single Si-based photodetector model had similar variations of spatial uniformity across their active areas.

Table 171G All Nine Photodetectors: Uniformity of Response to Light with Near Peak Responsivity Wavelength

Photodetector Measured	Plot of Response Across the Sensor Area to Light of the Indicated Wavelength		Typical Responsivity Plots Measurement Wavelength Indicated
GaP-Based Photodetector SM05PD7A: Mounted Photodiode FGAP71			
Si-Based Photodetectors SM05PD2A: Mounted Photodiode FDS010 and SM1PD2A			
Si-Based Photodetectors SM05PD1A: Mounted Photodiode FDS100 and SM1PD1A: Mounted Photodiode FDS1010			
InGaAs-Based Photodetectors SM05PD5A: Mounted Photodiode FGA21 and SM05PD4A: Mounted Photodiode FGA10			

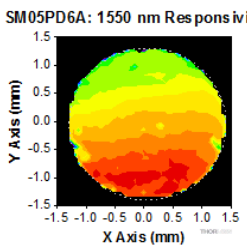
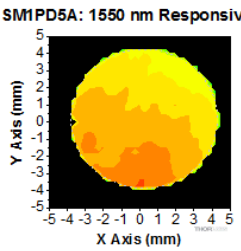
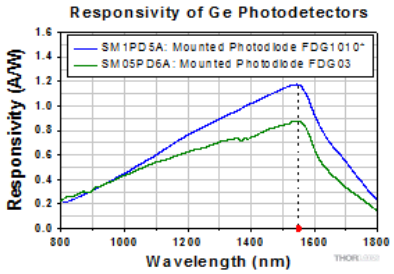
Ge-Based Photodetectors SM05PD6A: Mounted Photodiode FDG1010 and SM1PD5A: Mounted Photodiode FDG03			

Table 171H Selected Si-, InGaAs-, and Ge-Based Photodetectors: Uniformity of Response of Each to Three Different Wavelengths of Light

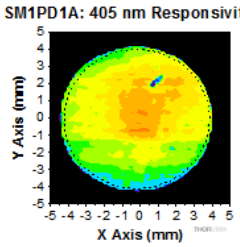
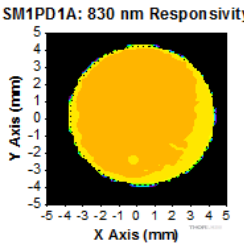
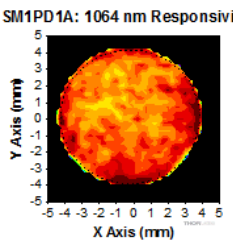
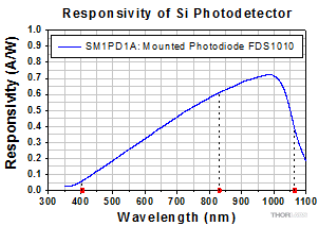
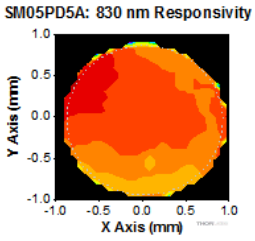
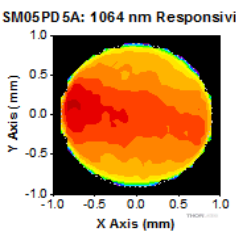
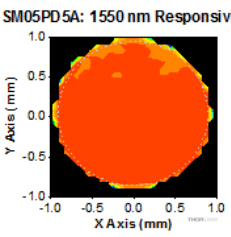
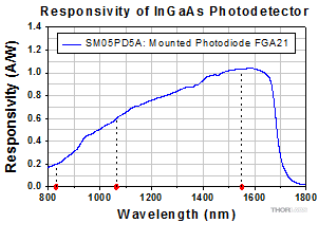
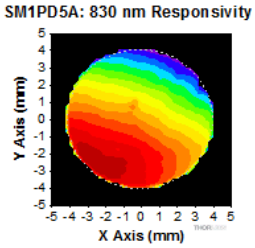
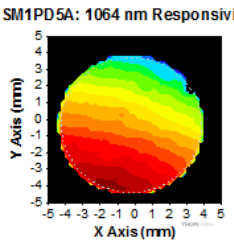
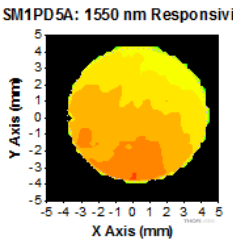
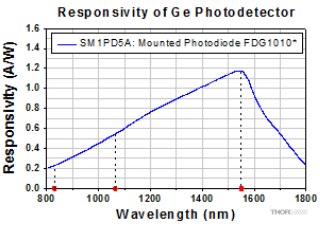
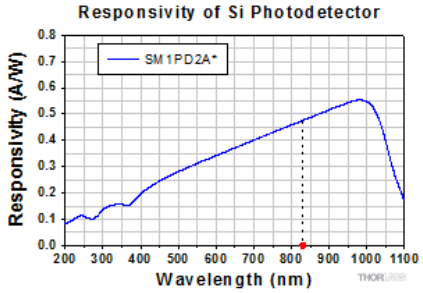
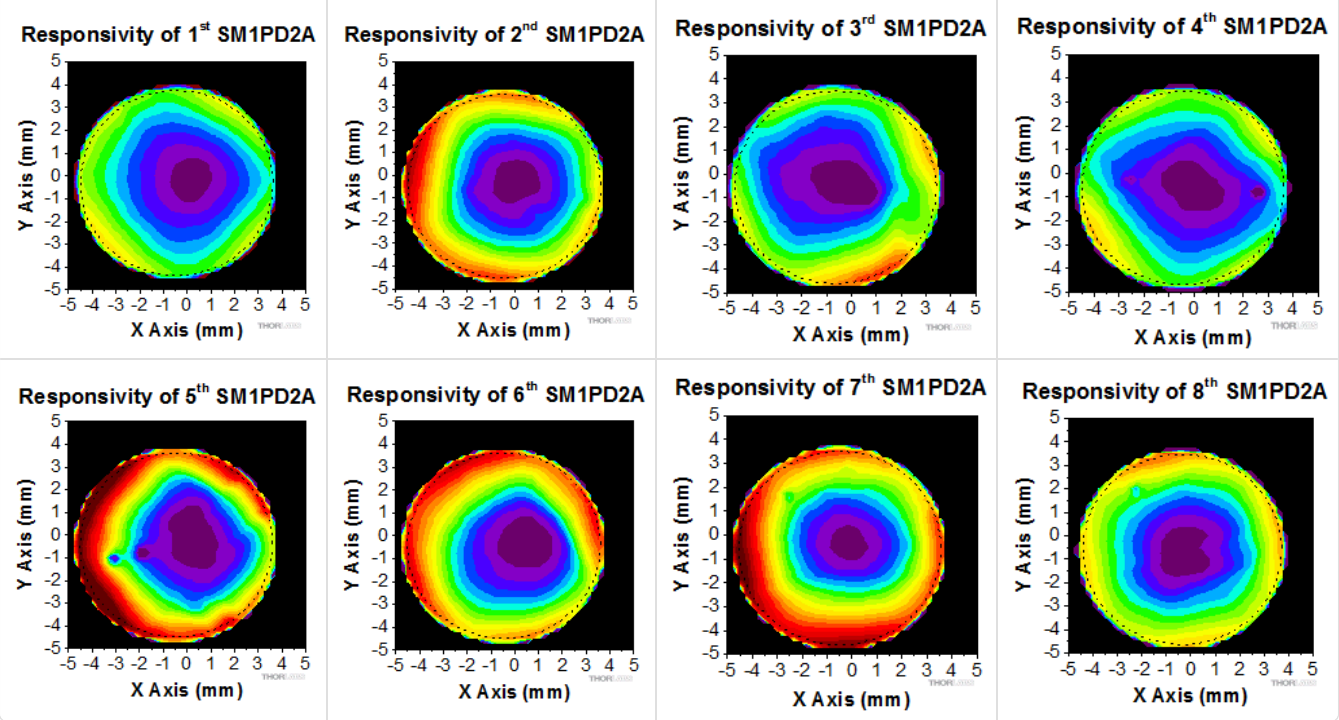
Photodetector	Plots of Response Across the Sensor Area to Light of the Indicated Wavelengths			Typical Responsivity Plots Measurement Wavelengths Indicated
Si-Based Photodetector SM1PD1A: Mounted Photodiode FDS1010				
InGaAs-Based Photodetector SM05PD5A: Mounted Photodiode FGA21				
Ge-Based Photodetector SM1PD5A: Mounted Photodiode FDG1010				

Table 171J Eight Si-Based SM1PD2A Photodetectors: Uniformity of Response to Light Near Peak Responsivity Wavelength Compared

Eight different Si-based SM1PD2A photodetectors were measured to compare the unit-to-unit variation of the response across the active area. Measurements were performed using 830 nm light, which is close to the wavelength of peak responsivity, as is indicted on the plot.	



References

[1] G. P. Agrawal, *Fiber-Optic Communication Systems*, 2nd ed., John Wiley & Sons, Inc., New York, 1997. (Particularly Chapter 4)
[2] A. Rogalski, K. Adamiec, and J. Rutkowski, *Narrow-Gap Semiconductor Photodiodes*, SPIE Press, Bellingham, WA, 2000.

Dark Current as a Function of Temperature

Measurements of dark current as a function of temperature were acquired for several unmounted photodetectors. As is described in the following section, dark current is a relatively small electrical current that flows in p-n junction photodetectors when no light is incident on the detector. Measurements were taken for silicon (Si), germanium (Ge), gallium phosphide (GaP), and indium gallium arsenide (InGaAs) reverse-biased photodiodes over temperatures from 25 °C to approximately 55 °C.

Current-Voltage Characteristics of p-n Junction Photodiodes

The characteristic current-voltage relationship of p-n junction photodiodes, as diagrammed in Figure 171K, possesses forward-biased and reverse-biased voltage regimes. In the reverse-biased voltage regime, in which p-n junction photodiodes are operated, a potential difference applied across the diode resists the flow of current. Ideally, if no light is incident on a reverse-biased photodiode, no current flows.

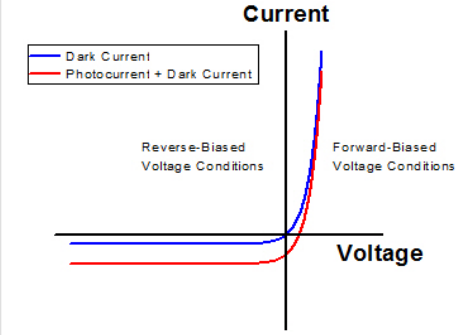


Figure 171K Current-Voltage Characteristic of a P-N Junction

Under real-world conditions, random processes in the semiconductor material of the photodiode always generates current carriers (electrons and holes) that produce current. These current generation processes are not driven by the photogeneration of electrons and holes. Instead, they are largely driven by the thermal energy contained in the semiconductor material.[1] This dark current is generally small, but it is present when the photodiode is reverse biased and not illuminated. Dark current magnitudes vary for photodiodes of different material compositions; the efficiencies of the thermal generation processes depend on the type and crystal quality of the semiconductor used in the detector's sensing head. The magnitude of the dark current can be expected to increase as the temperature of the photodiode increases.

When a photodiode is illuminated, the current generated by the incident light adds to the dark current. The carriers in the photocurrent are generated by the energy contained in the photons of the incident light. Above a certain illumination threshold intensity, the magnitude of the photocurrent exceeds the magnitude of the dark current. When the photocurrent is larger than the dark current, the magnitude of the photocurrent can be calculated by measuring the total current and then subtracting the contribution of the dark current. When the photocurrent is smaller than the dark current, the photocurrent is undetectable. Because of this, it is desirable to minimize the levels of dark current in photodiodes.

For convenience, both dark current and photocurrent are discussed as being independent of voltage over a range of voltages when the photodiode is reverse biased; however, the current flowing in real-world reverse-biased photodetectors is not completely independent of voltage over any voltage range. Regardless of whether the diode is illuminated, the current will increase as the magnitude of the reverse-bias voltage increases. In

addition, if the reverse-bias voltage is increased beyond a certain threshold, the photodiode will suffer reverse breakdown, in which the magnitude of the current increases exponentially and permanent damage to the diode is likely.

Experiment: Dark Currents Measured for Packaged Photodiodes

Dark currents were measured over temperatures of 25 °C to approximately 55 °C for four representative unpackaged photodiodes: the Si-based FDS1010, the Ge-based FDG50, the GaP-based FGAP71 (previous generation), and the InGaAs-based FGA10.

Experimental Setup

The experimental setup was designed to ensure a constant reverse-bias voltage across the photodiode, control the temperature of the detector, block light from reaching the detector, and establish an electrical path between the detector and the Keithley 6487 ammeter that isolated the measured current from extraneous electromagnetic interference (EMI) noise sources. Dark currents for these detectors can be on the order of nA, which made it important to control these conditions to ensure accurate measurements.

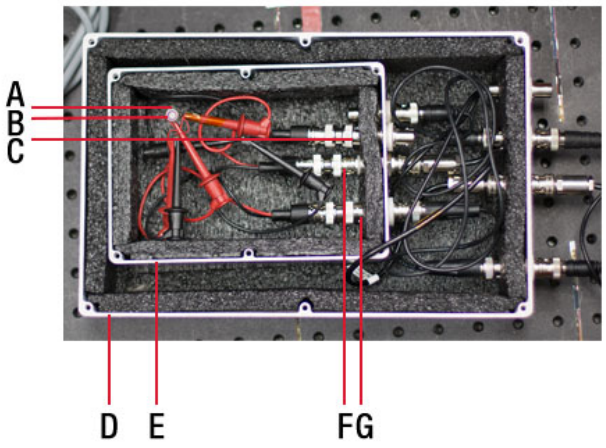


Figure 171L The Nested Metal Box Test Fixture with Covers Removed and FGA10 Installed
Black insulating foam lines the interiors of both boxes.
A: Thermistor; B: FGA10; C: BNC-to-BNC Feedthrough; D: Outer Box; E: Inner Box; F: BNC-to-Triax Feedthrough; G: BNC-to-BNC Feedthrough

The detector enclosure consisted of a pair of nested aluminum metal boxes, which are shown with their covers off in Figure 171L. Only one box would be required to create a light-tight environment for the photodiode, but an outer box was included in the setup to shield the inner box from EMI. The detector was placed inside the inner box, and it was electrically connected to the Keithley 6487 ammeter. The ammeter provided the required 5 V reverse-bias and received the output current signal. The electrical signals between the ammeter and the photodiode were routed through the two boxes using a combination of cables and feedthroughs. The 5 V bias voltage was connected to the photodiode using coax cables and BNC-to-BNC feedthroughs in the walls of both metal boxes. The current signal from the photodiode was connected to the BNC end of a BNC-to-Triax feedthrough integrated into the wall of the inner box. The signal was then routed through the outer box and to the Keithley 6487 using triax cables and a Triax-to-Triax feedthrough in the outer box. Triax cables were used because coax cables are poorly shielded, and using a coax cable to route the signal to the ammeter could introduce noise from EMI sources to the signal read from the detector. As the outer box shields the inner box from EMI, the noise introduced on the signal as it travels from the detector to the BNC-to-Triax feedthrough is mitigated.

Thermistors were used to monitor the temperatures of each photodiode continuously during the experiment. A piece of thermal tape was used to hold the thermistor flush against the TO cans of the FDG50, FGAP71, and the FGA10 during testing. The photosensor of the FDS1010 is mounted on a ceramic substrate, and when it was tested the thermistor was taped to the back of the substrate. The electrical connection between the thermistor and TSP01 temperature logger was performed using BNC cables, BNC-to-BNC bulkhead feedthroughs to route the signal out of the nested boxes, and a custom BNC-to-phono jack cable to connect to the temperature logger.



Figure 171M The Test Setup
The custom-built temperature chamber is on the top of the cart, and the temperature control instrumentation that includes the PRO8000 and TED8040 cards is on the cart's lower shelf.

A custom temperature chamber based on a XE25C9 standard enclosure was used to conduct these tests. It is shown on top of the cart in Figure 171M. The enclosure had a floor and four walls, and insulation was attached to all inner and outer surfaces. A lid for the enclosure was fashioned from a sheet of hardboard bordered with XE25 rails, and insulation was attached to the inner surface of the hardboard. Six resistive foil heaters were affixed to the walls of the XE25C9 enclosure, and they were driven using the PRO8000 fitted with six TED8040 thermoelectric cooler (TEC) controller cards placed on the bottom shelf of the cart in Figure 171M. Each TED8040 was interfaced with a heater and a thermistor installed in the chamber. The reading from the thermistor determined the current sent to drive the heater. The chamber was not actively cooled; cooling was instead performed by withdrawing the current driving the heaters and, as an option, opening the lid of the chamber.

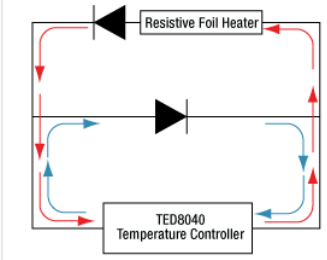


Figure 171N An electrical circuit that included a resistive foil heater, TED8040 temperature controller, and two rectifying diodes controlled current flow through the resistive current heater as described in the text.

The TED8040 units are designed to be interfaced with TECs, which produce heat when current flows in one direction, and which provide cooling when the current flows in the opposite direction. Because of this, when the enclosure exceeded the setpoint temperature, the TED8040 units in this experimental setup did not cut off the driving current. They instead reversed the current flow in an effort to produce cooling. In contrast to TECs, resistive foil heaters generate heat regardless of the direction of current flowing through them. In order to divert the driving current from the heaters, an electrical circuit, diagrammed in Figure 171N, that included two rectifying diodes was designed and implemented. Rectifying diodes allow current to flow only in one direction. When the temperature reading from the thermistor was lower than the setpoint temperature, current flowed in the direction of the red arrows and through the resistive heater, and heat was generated. When the temperature of the enclosure exceeded the setpoint temperature, the TED8040 controllers reversed the direction of

the current, so that it flowed in the direction of the blue arrows. Under this condition, the circuit diverted the current from the heaters and the chamber was allowed to cool.

Experimental Results

The data curves plotted in Figure 171P are the dark currents measured for the Si-based FDS1010, the Ge-based FDG50, the GaP-based FGAP71, and the InGaAs-based FGA10. Data were acquired continuously while the temperature was between 25 °C and 55 °C (shaded region of Figure 171Q). Figure 171Q is representative of the temperature measured at the photodiode during the experiment. The temperature profile included an initial segment of increasing temperature, followed by a soak that allowed the photodiode to reach the maximum temperature, and concluded with a cool-down. The data plotted in Figure 171P include all dark current measurements measured between 25 °C and 55 °C; current measurements taken at the same temperature, but at different times, overlay one another for each diode.

The data curves plotted in Figure 171P show that the measured dark current magnitudes differed depending on the material composing the photodiode. From lowest to highest:

- GaP-Based Detector FGAP71 (Lowest Dark Current)
- InGaAs-Based Detector FGA10
- Si-Based Detector FDS1010
- Ge-Based Detector FDG50 (Highest Dark Current)

These span approximately 6 orders of magnitude. In all cases, the dark current increased with the temperature of the photodiode, as expected. The individual points on this graph, plotted as diamonds, are the values of the dark current specified for each detector at 25 °C. These points specify a maximum value of dark current at 25 °C; each diode's dark current must be equal to or less than this value at 25 °C, but the dark current may exceed this specification at higher temperatures, as is the case for all but the measured FDS1010 detector.

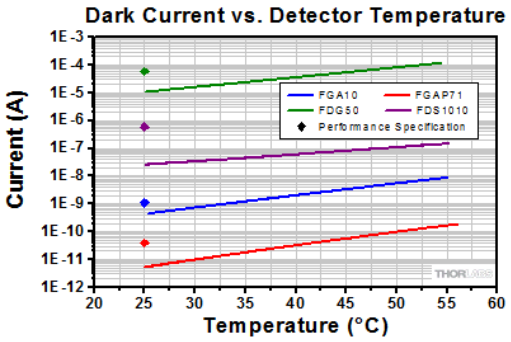


Figure 171P Dark Current Data Measured for Four Unmounted Photodiodes
The discrete data points, plotted as diamonds, are values of the dark current specified for each detector at 25 °C.

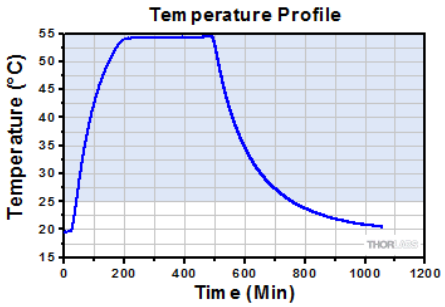


Figure 171Q Temperature of a Representative Photodiode Controlled by the Conditions in the Environmental Chamber
Dark current measurements were acquired between 25 °C and 55 °C (indicated by the shaded region) and are plotted in Figure 171P.

Experimental Limitations

Measurements were performed using a single representative of each detector type, as these data were intended to illustrate overall trends. These data should not be taken as specific for a particular diode. The measured dark current is a function of voltage bias, temperature dependence of resistive loads, and other effects. Efforts were made to suppress their influence on these measurements, including using the Keithley 6487 ammeter to provide the required 5 V reverse bias. Using the ammeter removed the need to use a load resisitor, which may exhibit its own temperature dependence. The thermistor was placed as close to the semiconductor sensor as was possible, but it was not placed in direct contact with the sensor. Because of this, there may have been a difference between the measured temperature and the temperature of the semiconductor material. The dark current was measured while the temperature of the environmental chamber was continuously varied. Humidity was not controlled during this experiment.

[1] J. Liu, Photonic Devices. Cambridge University Press, Cambridge, UK, 2005

Noise Equivalent Power (NEP) as a Function of Temperature

Noise Equivalent Power (NEP) was determined as a function of temperature for several unmounted photodetectors. As is described in the following section, NEP is a common metric used to describe the minimum sensitivity of a photodetector. Measurements were taken for silicon (Si), germanium (Ge), gallium phosphide (GaP), and indium gallium arsenide (InGaAs) reverse-biased photodiodes over temperatures from 25 °C to approximately 55 °C.

Noise Equivalent Power

The most general definition of NEP is "the input signal power that results in a signal-to-noise ratio (SNR) of 1 in a 1 Hz output bandwidth." [1] Therefore, in order to determine the NEP, the minimum noise of the photodiode must be determined. When the optical signal is blocked, noise is still present, which is generated by the detector itself. There are two main contributors to photodiode noise: the shot noise due to dark current and thermal noise due to the shunt resistance.

Dark current is a relatively small electric current present in photosensitive devices that flows through the device, including when there is no incident light. More information on the dark current can be found in the "Dark Current as a Function of Temperature" section above. Shot noise is due to the quantized nature of the charge carriers. For the case where there is no light incident on the detector, it can be calculated from the dark current of the detector using the equation [2]

$$i_S = \sqrt{2qI_D f_{BW}}$$

where i_s is the shot noise, I_d is the dark current, q is the electron charge, and f_{BW} is the bandwidth, which will be set to 1 Hz to allow for comparison between different photodiodes.

Thermal, or Johnson, noise is due to the random thermal motion of the charge carriers. Thermal noise will be generated only by the resistive elements of the system. For the photodiode detector, the shunt resistance needs to be considered. Shunt resistance is the resistance of the zero-biased photodiode p-n junction; put another way, it is the inverse of the slope of the IV curve at the zero-voltage point. Since it is difficult to correctly calculate the slope at the zero crossing, the generally accepted industry practice is to measure the current at V = ±10 mV and then calculate the slope. Then the thermal noise due to the shunt resistance, R_{SH}, can be expressed as:

$$i_T = \sqrt{\frac{4k_B T}{R_{SH}} f_{BW}}$$

where i_t is the thermal noise (expressed as a current), k_B is Boltzmann's constant, T is temperature, R_{SH} is shunt resistance, and f_{BW} is the bandwidth.

The total noise, i_{total}, is the quadrature sum of all noise sources:

$$i_{total} = \sqrt{i_S^2 + i_T^2}$$

Note that this result is the total noise expressed for the current output of the photodiode, while the NEP is expressed in terms of incident optical power. Thus, to compare with the NEP specifications a typical responsivity value, $\Re$, is chosen for the specified wavelength:

$$NEP = \frac{i_{total}}{\Re}$$

Also, to allow for comparison between different diodes, we set the bandwidth to 1 Hz for the calculation.

Experiment: Dark Current and Shunt Resistance Measurements

NEP was determined over 25 to 55 °C for four representative unpackaged photodiodes: the Si-based FDS1010, the Ge-based FDG50, the GaP-based FGAP71 (previous generation), and the InGaAs-based FGA10.

Experimental Setup

The experimental setup was designed to ensure a constant reverse-bias voltage across the photodiode, control the temperature of the detector, block light from reaching the detector, and establish an electrical path between the detector and the Keithley 6487 ammeter that isolated the measured current from extraneous electromagnetic interference (EMI) noise sources. Dark currents for these detectors can be on the order of nA, which made it important to control these conditions to ensure accurate measurements.

The detector enclosure consisted of a pair of nested aluminum metal boxes, which are shown with their covers off in Figure 171R. Only one box would be required to create a light-tight environment for the photodiode, but an outer box was included in the setup to shield the inner box from EMI. The detector was placed inside the inner box, and it was electrically connected to the Keithley 6487 ammeter. The ammeter provided the required

reverse-bias voltage and received the output current signal. The electrical signals between the ammeter and the photodiode were routed through the two boxes using a combination of cables and feedthroughs. The bias voltage was connected to the photodiode using coax cables and BNC-to-BNC feedthroughs in the walls of both metal boxes. The current signal from the photodiode was connected to the BNC end of a BNC-to-Triax feedthrough integrated into the wall of the inner box. The signal was then routed through the outer box and to the Keithley 6487 using triax cables and a Triax-to-Triax feedthrough in the outer box. Triax cables were used because coax cables are poorly shielded, and using a coax cable to route the signal to the ammeter could introduce noise from EMI sources to the signal read from the detector. As the outer box shields the inner box from EMI, the noise introduced on the signal as it travels from the detector to the BNC-to-Triax feedthrough is mitigated.

For dark current measurements, the bias voltage was set to 5 V. In order to calculate the shunt resistance, measurements of the current were made with the bias voltage set to +10 mV and -10 mV.

Thermistors were used to monitor the temperatures of each photodiode continuously during the experiment. A piece of thermal tape was used to hold the thermistor flush against the TO cans of the FDG50, FGAP71, and the FGA10 during testing. The photosensor of the FDS1010 is mounted on a ceramic substrate, and when it was tested the thermistor was taped to the back of the substrate. The electrical connection between the thermistor and TSP01 temperature logger was performed using BNC cables, BNC-to-BNC bulkhead feedthroughs to route the signal out of the nested boxes, and a custom BNC-to-phono jack cable to connect to the temperature logger.

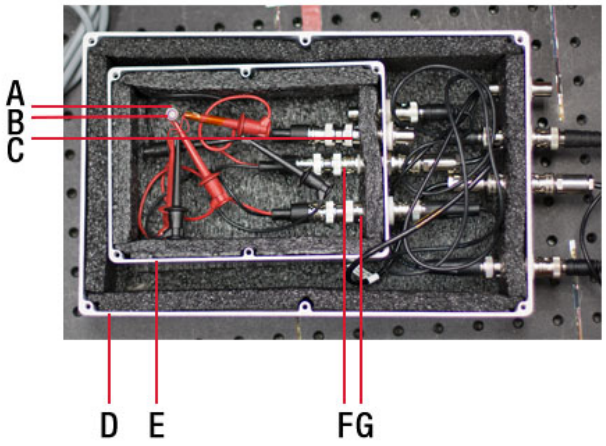


Figure 171R The nested metal box test fixture with covers removed and FGA10 installed.
Black insulating foam lines the interiors of both boxes.
A: Thermistor; B: FGA10; C: BNC-to-BNC Feedthrough; D: Outer Box; E: Inner Box; F: BNC-to-Triax Feedthrough; G: BNC-to-BNC Feedthrough

A custom temperature chamber based on a XE25C9 standard enclosure was used to conduct these tests. It is shown on top of the cart in Figure 171U. The enclosure had a floor and four walls, and insulation was attached to all inner and outer surfaces. A lid for the enclosure was fashioned from a sheet of hardboard bordered with XE25 rails, and insulation was attached to the inner surface of the hardboard. Six resistive foil heaters were affixed to the walls of the XE25C9 enclosure, and they were driven using the PRO8000 chassis fitted with six TED8040 thermoelectric cooler (TEC) controller cards placed on the bottom shelf of the cart in Figure 171T. Each TED8040 was interfaced with a heater and a thermistor installed in the chamber. The reading from the thermistor determined the current sent to drive the heater. The chamber was not actively cooled; cooling was instead performed by withdrawing the current driving the heaters and, as an option, opening the lid of the chamber.



Figure 171T The Test Setup
The custom-built temperature chamber is on the top of the cart, and the temperature control instrumentation that includes the PRO8000 and TED8040 cards is on the cart's lower shelf.

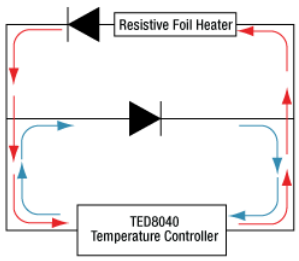


Figure 171U An electrical circuit that included a resistive foil heater, TED8040 temperature controller, and two rectifying diodes controlled current flow through the resistive current heater as described in the text.

The TED8040 units are designed to be interfaced with TECs, which produce heat when current flows in one direction, and which provide cooling when the current flows in the opposite direction. Because of this, when the enclosure exceeded the setpoint temperature, the TED8040 units in this experimental setup did not cut off the driving current. They instead reversed the current flow in an effort to produce cooling. In contrast to TECs, resistive foil heaters generate heat regardless of the direction of current flowing through them. In order to divert the driving current from the heaters, an electrical circuit, diagrammed in Figure 171U, that included two rectifying diodes was designed and implemented. Rectifying diodes allow current to flow only in one direction. When the temperature reading from the thermistor was lower than the setpoint temperature, current flowed in the direction of the red arrows and through the resistive heater, and heat was generated. When the temperature of the enclosure exceeded the setpoint temperature, the TED8040 controllers reversed the direction of the current, so that it flowed in the direction of the blue arrows. Under this condition, the circuit diverted the current from the heaters and the chamber was allowed to cool.

Experimental Results

The data curves plotted in Figure 171W are the dark currents measured for the Si-based FDS1010, the Ge-based FDG50, the GaP-based FGAP71, and the InGaAs-based FGA10. Figure 171X shows the calculated shunt resistance values for the same diodes as Figure 171W. Data were acquired continuously while the temperature was between 25 °C and 55 °C (shaded region of Figure 171Z). Figure 171Z is representative of the temperature measured at the photodiode during the experiment. The temperature profile included an initial segment of increasing temperature, followed by a soak that allowed the photodiode to reach the maximum temperature, and concluded with a cool-down. The data plotted in Figures 171W and 171X include all dark current measurements measured between approximately 25 °C and 55 °C; current measurements taken at the same temperature, but at different times, overlay one another for each diode.

As shown in Figure 171X, the shunt resistance for the measured GaP, InGaAs, and Si detectors is relatively large; therefore in many situations it can be ignored. For the Ge-based FDG50 the shunt resistance is relatively low, especially at higher temperatures. For this diode the shunt resistance

might need to be considered if there is a high load involved.

Figure 171Y shows the calculated NEP vs. temperature for each diode. Since the NEP is a function of responsivity, which varies with wavelength, the NEP values are calculated at the peak responsivity value as given in Table 171V.

The data curves plotted in Figure 171Y show that the calculated NEP magnitudes differed depending on the material composing the photodiode. From lowest to highest:

- GaP-Based Detector FGAP71 (Lowest NEP)
- InGaAs-Based Detector FGA10
- Si-Based Detector FDS1010
- Ge-Based Detector FDG50 (Highest NEP)

Table 171V Responsivity Used for NEP Calculation	
FGA10	1.05 A/W @ 1550 nm
FDG50	0.85 A/W @ 1550 nm
FGAP71	0.12 A/W @ 440 nm
FDS1010	0.725 A/W @ 970 nm

These span approximately 6 orders of magnitude. In all cases, the dark current increased with the temperature of the photodiode, as expected. The individual points on this graph, plotted as diamonds, are the values of the dark current specified for each detector at 25 °C. These points specify a maximum value of dark current at 25 °C; each diode's dark current and NEP must be equal to or less than this value at 25 °C, but the dark current and NEP may exceed this specification at higher temperatures.

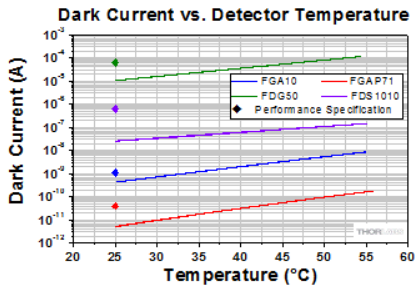


Figure 171W Dark Current Data Measured for Four Unmounted Photodiodes
The discrete data points, plotted as diamonds, are values of the dark current specified for each detector at 25 °C.

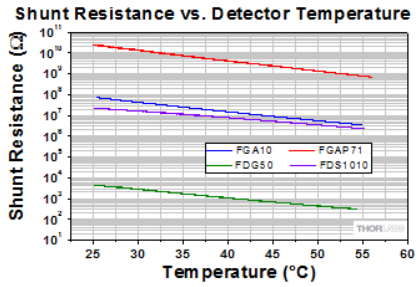


Figure 171X Shunt Resistance Calculated as Described in the Text for Four Unmounted Photodiodes

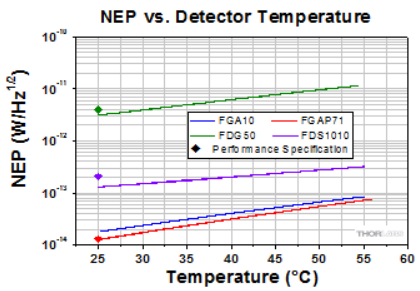


Figure 171Y NEP Calculated from the Quadrature Sum of Shot Noise and Thermal Noise for Four Unmounted Photodiodes
The discrete data points, plotted as diamonds, are values of the NEP specified for each detector at 25 °C. There is no point for FGA10 since the NEP is not specified at the peak responsivity wavelength.

Experimental Limitations

Measurements were performed using a single representative of each detector type, as these data were intended to illustrate overall trends. These data should not be taken as specific for a particular diode. The measured currents were functions of voltage bias, temperature dependence of resistive loads, and other effects. Efforts were made to suppress their influence on these measurements, including using the Keithley 6487 ammeter to provide the required 5 V reverse bias. Using the ammeter removed the need to use a load resistor, which may exhibit its own temperature dependence. The thermistor was placed as close to the semiconductor sensor as was possible, but it was not placed in direct contact with the sensor. Because of this, there may have been a difference between the measured temperature and the temperature of the semiconductor material. The currents were measured while the temperature of the environmental chamber was continuously varied. Humidity was not controlled during this experiment.

[1] Thorlabs' Noise Equivalent Power White Paper.

[2] Quimby, Richard S. Photonics and Lasers: An Introduction. Wiley-Interscience, Hoboken, NJ, 2006, pp 241-244.

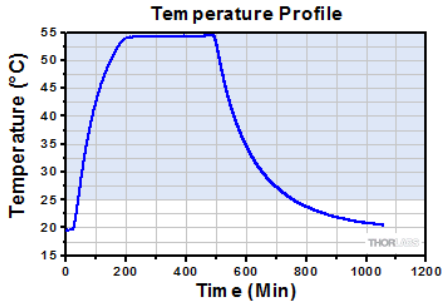


Figure 171Z Temperature of a Representative Photodiode Controlled by the Conditions in the Environmental Chamber
Dark current measurements were acquired between 25 °C and 55 °C (indicated by the shaded region) and are plotted in Figure 171X.

Beam Size and Photodiode Saturation

We present laboratory measurements showing the effect of beam size on the saturation point of a Thorlabs silicon photodiode. As defined here, saturation is a 1% deviation from the linear response region. As illustrated in Figure 171AA, the photodiode saturated at lower incident power levels as the beam size decreased. Several additional calculations and experiments were performed to verify the cause of the change in saturation was not a function of the power density. These results suggest that users should be cognizant of the beam size when attempting to measure absolute power with a power sensor, such as our S130C photodiode power sensor.

For our experiment, we used the SM1PD1A mounted photodiode, which consists of an FDS1010 photodiode in an SM1-threaded housing. An 830 nm superluminescent diode was used as the light source. A beamsplitter directed 20% of the light to a monitor photodiode while the remainder was transmitted through a focusing lens. Power values were calibrated using an integrating sphere, while the beam size of the focusing beam was calibrated with a beam profiler mounted to a translation stage. After calibration, the beam profiler was replaced with the device under test (DUT), an SM1PD1A at a 0 V bias. The output current was measured with an ammeter to remove the need for a load resistor. We then recorded datasets as the beam diameter was continuously scanned from 0.06 mm to 5 mm while power was held constant, as well as measurements for beam diameters ranging from 1 mm to 5 mm (measured to the 5% clip level) as the incident power was continuously scanned from 0.12 mW to 5 mW.

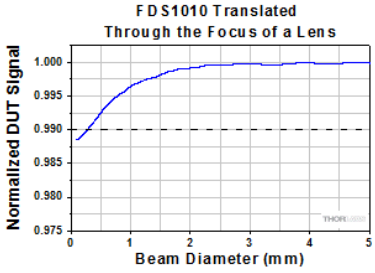


Figure 171AA Normalized change in output current for a fixed incident power as the photodiode Device Under Test (DUT), FDS1010, was translated through the focus of a lens.

The figures show the results from the measurements. Figure 171AA and Figure 171AB show the deviation from linear response for continuously varying beam diameter at a fixed 1 mW incident power (Figure 171AA) and continuously varying incident power for several beam diameters (Figure 171AB). Figure 171AA shows that for a 1 mW input, the photodiode saturated at beam sizes less than 300 µm. Figure 171AB shows that beam diameters ≥2 mm did not saturate at the power levels investigated.

Lab Facts

Click for Full Lab Facts Summary

One hypothesis for these results was that local saturation due to a large power density locally depleted or reduced the population of available carriers. In Figure 171AC, we calculated the power density by taking the quotient of the measured power and beam diameter presented in Figure 171AB and plotted the current output as a function of that power density. If the results were due to local saturation, we would have expected that all of the beam diameters would saturate at a single power density; however, this was not the case.

Since the results presented in Figure 171AC coupled the beam size change with a change in optical power density, we performed another experiment to increase the power density incident on the sensor within the same envelope of beam area to see if there was a change in the saturation point. This was done by segmenting the Gaussian beam into an array of beamlets with a microlens array, concentrating the overall optical power into smaller spots within the same Gaussian envelope. This created larger power densities while maintaining a similar electrical path to the sensor leads. Figure 171AD shows the same results as Figure 171AB with the results from the microlens array overlaid as dashed lines. Since the results are nearly identical to the original Gaussian beam for all diameters, the saturation appears to be dependent on the overall beam diameter and independent of the power density. In the complete Lab Facts presentation, we discuss how these results support the theory of Scholze *et al.* that the change in saturation with beam size is due to a change in the series resistance of the photodiode [1].

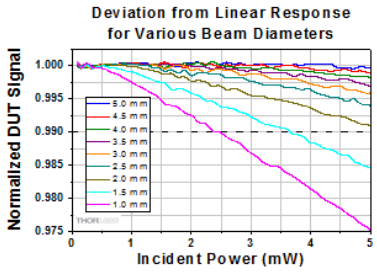


Figure 171AB Percent Deviation from the linear response with increasing power for 1 mm - 5 mm beam diameters. The 1% deviation level is indicated with a dashed horizontal line.

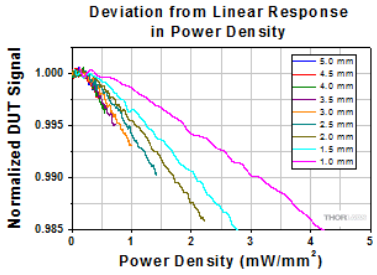


Figure 171AC Normalized output current versus power density for 1 mm - 5 mm beam diameters. This shows the saturation effects do not appear to be based on a single power density.

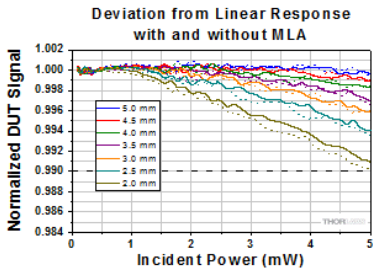


Figure 171AD Normalized output current versus optical power for 2 mm - 5 mm beam diameter with (Dashed Line) and without (Solid Line) the microlens array (MLA) prior to the photodiode.

[1] F. Scholze, R. Klein, R. Muller, Linearity of silicon photodiodes for EUV radiation. 2004 Proc. SPIE 5374 926–34.

Effective Reverse Bias Voltage as a Function of Incident Optical Power

Introduction

Lab Facts

Click for Full Lab Facts Summary

The bandwidth (and rise time) of a photodiode is known to be a function of the effective bias across it. Therefore, the effective bias must be tuned in response to the generated photocurrent from the optical power incident on the diode to maintain the desired bandwidth. This lab fact investigates the relationship between the effective reverse bias voltage across a photodiode and the CW optical power incident on it in order to create a reliable model of a biased photodiode.

Circuit Analysis

To begin creating this model, the photodiode circuit shown in Figure 171AF is examined using Ohm's law and assuming a constant DC voltage source; this yields the equation

$$V_{eff} = V_0 - i_{PD} * (R_P + R_L). \quad (1)$$

The effective bias voltage (V_{eff}) across the photodiode equals the initial voltage from the source (V_0) minus the product of the photocurrent (i_{PD}) and the sum of the resistance of the bias module's resistor (R_P) and the load resistor (R_L).

To find how V_{eff} changes with respect to the incident optical power (P), i_{PD} is replaced in Equation 1 with its definition as the product of the wavelength-dependent responsivity [$\Re(\lambda)$] of the photodiode and P:

$$i_{PD} = \Re(\lambda) * P. \quad (2)$$

Using Ohm's law on the load resistor such that $i_{PD} = V_L / R_L$, Equation 2 was rewritten to solve for $\Re(\lambda)$:

$$\Re(\lambda) = V_L / (P * R_L). \quad (3)$$

Assuming that the voltage drop across the load resistor (V_L) is linear with respect to increasing P, the ratio of the change in V_L and P can be established as the ratio:

$$m = \Delta V_L / \Delta P. \quad (4)$$

These equations can be combined to form:

$$V_{eff} = V_0 - (m / R_L) * P * (R_P + R_L). \quad (5)$$

The ratio m can be calculated from empirical measurements of V_L and P for each photodiode, allowing this equation to be used as a model for how V_{eff} changes with respect to P.

Experiment

An experiment was developed to measure the change in V_L with respect to changes in P. Output from a fiber-coupled laser diode was collimated, passed through a neutral density filter, and then focused onto the Device Under Test (DUT) via an off-axis parabolic mirror. A photograph of the setup used can be seen in Figure 171AE. Neutral density filters with a range of optical densities were used to vary the power incident on the photodiode. For each photodiode used, the distance between the sensor surface and focusing mirror was adjusted so that the spot size was approximately half the size of each photodiodes' detector area. An oscilloscope was used to measure V_0, V_L, and the sum $V_{eff} + V_L$. A multimeter was used to measure the effective bias directly.

Results

V_L was plotted against P for each DUT; an example of the results for the silicon photodiode can be seen in Figure 171AG. A linear trend line was created for each data set, and the slope of that line corresponds to m in Equation 4. This value can be used in Equation 5 to calculate the effective bias voltage. Then, V_{eff} can be plotted with respect to the incident power and compared to the measured values from the oscilloscope. These results are shown in the three graphs displayed in Figures 171AH, 171AJ, and 171AK. The model was found to be consistent with measured experimental results, which showed that V_{eff} decreases as P increases (with V_0, R_P, and R_L held constant). This effect is significant, because the voltage set at the voltage source is not necessarily the bias voltage applied to the photodiode; one must account for resistive components within the circuit to calculate the effective bias voltage applied across the photodiode.

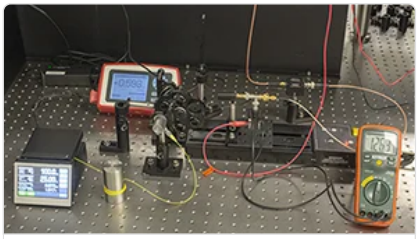


Figure 171AE This setup was used in the experiment in order to verify our model of the effective voltage across the photodiode.

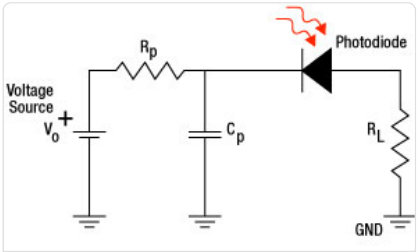


Figure 171AF Circuit Diagram of Biased Photodiode

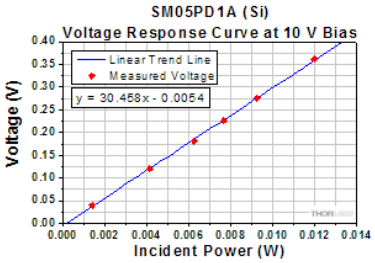


Figure 171AG A single voltage vs. incident power graph used to find m for the final model, Equation 5.

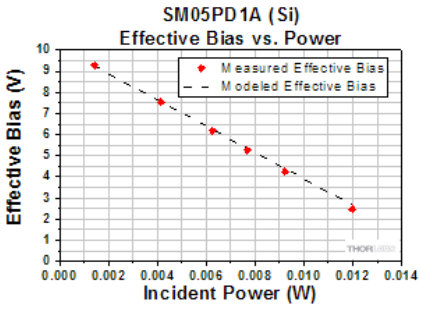


Figure 171AH Measured Effective Bias Values for SM05PD1A with Their Modeled Values

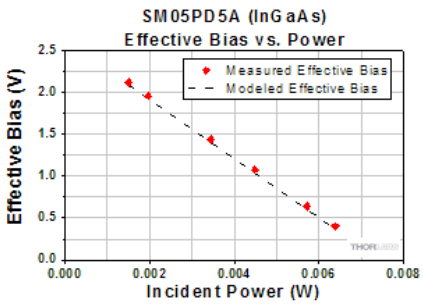


Figure 171AJ Measured Effective Bias Values for SM05PD5A with Their Modeled Values

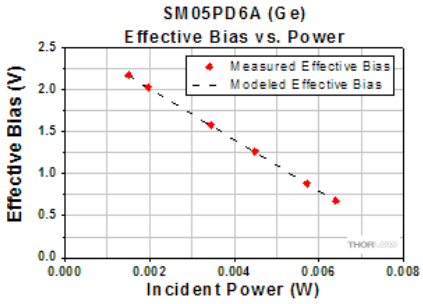
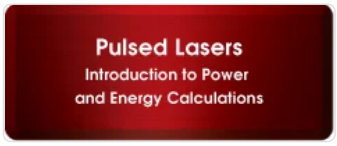


Figure 171AK Measured Effective Bias Values for SM05PD6A with Their Modeled Values

About Our Lab Facts

Our application engineers live the experience of our customers by conducting experiments in Alex's personal lab. Here, they gain a greater understanding of our products' performance across a range of application spaces. Their results can be found throughout our website on associated product pages in *Lab Facts* tabs. Experiments are used to compare performance with theory and explore the benefits and drawbacks of using similar products in unique setups, in an attempt to understand the intricacies and practical limitations of our products. In all cases, the theory, procedure, and results are provided to assist with your buying decisions.

Pulsed Laser Emission: Power and Energy Calculations



Determining whether emission from a pulsed laser is compatible with a device or application can require referencing parameters that are not supplied by the laser's manufacturer. When this is the case, the necessary parameters can typically be calculated from the available information. Calculating peak pulse power, average power, pulse energy, and related parameters can be necessary to achieve desired outcomes including:

- Protecting biological samples from harm.
- Measuring the pulsed laser emission without damaging photodetectors and other sensors.
- Exciting fluorescence and non-linear effects in materials.

Pulsed laser radiation parameters are illustrated in Figure 170A and described in Table 170B. For quick reference, a list of equations is provided below. The document available for download provides this information, as well as an introduction to pulsed laser emission, an overview of relationships among the different parameters, and guidance for applying the calculations.

Equations:

Period and *repetition rate* are reciprocal: $\Delta t = \frac{1}{f_{rep}}$ and $f_{rep} = \frac{1}{\Delta t}$

Pulse energy calculated from *average power*: $E = \frac{P_{avg}}{f_{rep}} = P_{avg} \cdot \Delta t$

Average power calculated from *pulse energy*: $P_{avg} = \frac{E}{\Delta t} = E \cdot f_{rep}$

Peak pulse power estimated from *pulse energy*: $P_{peak} \approx \frac{E}{\tau}$

Peak power and *average power* calculated from each other:

$$P_{peak} = \frac{P_{avg}}{f_{rep} \cdot \tau} = \frac{P_{avg} \cdot \Delta t}{\tau} \quad \text{and} \quad P_{avg} = P_{peak} \cdot f_{rep} \cdot \tau = \frac{P_{peak} \cdot \tau}{\Delta t}$$

Peak power calculated from *average power* and *duty cycle**:

$$P_{peak} = \frac{P_{avg}}{\tau/\Delta t} = \frac{P_{avg}}{duty\ cycle}$$

*Duty cycle ($\tau/\Delta t$) is the fraction of time during which there is laser pulse emission.

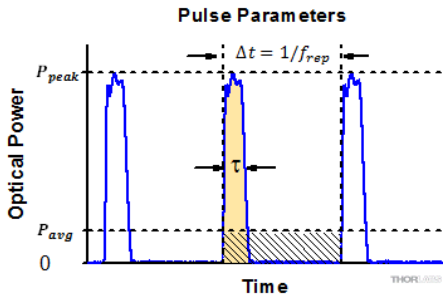


Figure 170A Parameters used to describe pulsed laser emission are indicated in this plot and described in Table 170B. **Pulse energy** (**E**) is the shaded area under the pulse curve. Pulse energy is, equivalently, the area of the diagonally hashed region.

Example Calculation:

Is it safe to use a detector with a specified maximum peak optical input power of **75 mW** to measure the following pulsed laser emission?

- Average Power: 1 mW
- Repetition Rate: 85 MHz
- Pulse Width: 10 fs

The energy per pulse:

$$E = \frac{P_{avg}}{f_{rep}} = \frac{1\ mW}{85\ MHz} = \frac{1\ x\ 10^{-3} W}{85\ x\ 10^{6} Hz} = 1.18\ x\ 10^{-11} J = 11.8\ pJ$$

seems low, but the peak pulse power is:

$$P_{peak} = \frac{P_{avg}}{f_{rep} \cdot \tau} = \frac{1\ mW}{85\ MHz \cdot 10\ fs} = 1.18\ x\ 10^{3}\ W = \mathbf{1.18\ kW}$$

It is ***not safe*** to use the detector to measure this pulsed laser emission, since the peak power of the pulses is >5 orders of magnitude higher than the detector's maximum peak optical input power.

Table 170B Pulse Parameters

Parameter	Symbol	Units	Description
Pulse Energy	E	Joules [J]	A measure of one pulse's total emission, which is the only light emitted by the laser over the entire period. The pulse energy equals the shaded area, which is equivalent to the area covered by diagonal hash marks.
Period	Δt	Seconds [s]	The amount of time between the start of one pulse and the start of the next.
Average Power	P_{avg}	Watts [W]	The height on the optical power axis, if the energy emitted by the pulse were uniformly spread over the entire period.
Instantaneous Power	P	Watts [W]	The optical power at a single, specific point in time.
Peak Power	P_{peak}	Watts [W]	The maximum instantaneous optical power output by the laser.
Pulse Width	τ	Seconds [s]	A measure of the time between the beginning and end of the pulse, typically based on the full width half maximum

Table 170B Pulse Parameters			
Parameter	Symbol	Units	Description
			(FWHM) of the pulse shape. Also called **pulse duration**.
Repetition Rate	f_{rep}	Hertz [Hz]	The frequency with which pulses are emitted. Equal to the reciprocal of the period.

Cross Reference

The following table lists Thorlabs' selection of photodiodes, photoconductive, and pyroelectric detectors. Item numbers in the same row contain the same detector element.

Photodetector Cross Reference

Wavelength	Material	Unmounted Detectors	Mounted Photodiode	Biased Detector	Amplified Detector	Amplified Detector, OEM Package
200 - 1100 nm	Si	FDS010	SM05PD2A SM05PD2B	DET10A2	PDA10A2	PDAPC5
	Si	-	SM1PD2A	-	-	-
0.2 - 25 µm	$LiTaO_3$		-	-	PDA20L2[e]	-
240 - 1170 nm	Black Si	FDBS11	SM05PD9A	DET10X2	PDA10X2	PDAPC11
	Black Si	FDBS22	SM05PD8A	DET20X2	PDA20X2	PDAPC10
	Black Si	FDBS25	-	-	-	-
320 - 1000 nm	Si	-	SM05PD11A	DET8A2	PDA8A2	-
320 - 1100 nm	Si	FD11A	SM05PD3A	-	PDF10A2	-
	Si	-[a]	-	DET100A2	PDA100A2	PDAPC2[a]
340 - 1100 nm	Si	FDS10X10	-	-	-	-
350 - 1100 nm	Si	FDS100 FDS100-CAL[b]	SM05PD1A SM05PD1B	DET36A2	PDA36A2	PDAPC1
	Si	FDS1010 FDS1010-CAL[b]	SM1PD1A SM1PD1B	-	-	-
400 - 1000 nm	Si	-	-	-	PDA015A2 FPD310-FS-VIS FPD310-FC-VIS FPD510-FC-VIS FPD510-FS-VIS FPD610-FC-VIS FPD610-FS-VIS	-
400 - 1100 nm	Si	FDS015[c]	-	-	-	-
	Si	FDS025[c] FDS02[d]	-	DET02AFC(/M) DET025AFC(/M) DET025A(/M) DET025AL(/M)	-	-
400 - 1700 nm	Si & InGaAs	DSD2	-	-	-	-
500 - 1700 nm	InGaAs	-	-	DET10N2	-	-
0.6 - 16 µm	$LiTaO_3$	EPD13[e]	-	-	PDA13L2[e]	-
750 - 1650 nm	InGaAs	-	-	-	PDA8GS	-
800 - 1700 nm	InGaAs	FGA015	SM05PD10A	-	PDA015C2	-
	InGaAs	FGA21 FGA21-CAL[b]	SM05PD5A	DET20C2	PDA20C2 PDA20CS2	-
	InGaAs	FGA01[c] FGA01FC[d]	-	DET01CFC(/M)	-	-
	InGaAs	FDGA05[c]	-	-	PDA05CF2	PDAPC6
	InGaAs	-	-	DET08CFC(/M) DET08C(/M) DET08CL(/M)	-	-
	InGaAs	-	-	-	PDF10C2	-
800 - 1800 nm	Ge	FDG03 FDG03-CAL[b]	SM05PD6A	DET30B2	PDA30B2	-
	Ge	FDG50	-	DET50B2	PDA50B2	PDAPC8
	Ge	FDG05	-	-	-	-
900 - 1700 nm	InGaAs	FGA10	SM05PD4A	DET10C2	PDA10CS2	-
900 - 2600 nm	InGaAs	FD05D	-	DET05D2	-	-
		FD10D	SM05PD12A	DET10D2	PDA10D2	PDAPC7

Photodetector Cross Reference						
Wavelength	Material	Unmounted Detectors	Mounted Photodiode	Biased Detector	Amplified Detector	Amplified Detector, OEM Package
950 - 1650 nm	InGaAs	-	-	-	FPD310-FC-NIR FPD310-FS-NIR FPD510-FC-NIR FPD510-FS-NIR FPD610-FC-NIR FPD610-FS-NIR	-
1.0 - 5.8 µm	InAsSb	-	-	-	PDA10PT(-EC)	-
2.0 - 8.0 µm	HgCdTe (MCT)	VML8T0[f] VML8T4[f,g]	-	-	PDAVJ8[f]	-
2.0 - 10.6 µm	HgCdTe (MCT)	VML10T0[f] VML10T4[f,g]	-	-	PDAVJ10[f]	-
2.7 - 5.0 µm	HgCdTe (MCT)	VL5T0[f]	-	-	PDAVJ5[f]	-
2.7 - 5.3 µm	InAsSb	-	-	-	PDA07P2	PDAPC9

a. If you are interested in purchasing the bare photodiode incorporated in these detectors without the printed circuit board, please contact Tech Support .
b. Calibrated Unmounted Photodiode
c. Unmounted TO-46 Can Photodiode
d. Unmounted TO-46 Can Photodiode with FC/PC Bulkhead
e. Pyroelectric Detector
f. Photovoltaic Detector
g. Internal Thermoelectric Cooling

Si Photodiodes - 200 nm to 1100 nm

Table G1.1 Specifications

Click Image for Details								
Item #	FDS010	FD11A	FDS10X10	FDS100	FDS1010	FDS015	FDS02	FDS025
Key Feature	High Speed, UV Grade Fused Silica Window to Provide Sensitivity Down to 200 nm	Lowest Dark Current in TO-18 Can with a Window	Low Dark Current in 10 mm x 10 mm Ceramic Package	High Speed, Largest Sensor in a TO-5 Can	High Speed, Large Active Area and Mounted on an Insulating Ceramic Substrate	Highest Speed and Lowest Capacitance in a TO-46 Can with an AR-Coated Window	High Speed and Low Capacitance in a Direct Fiber-Coupled FC/PC Package	High Speed and Low Capacitance in a TO-46 Can with a Ball Lens
Info	ⓘ	ⓘ	ⓘ	ⓘ	ⓘ	ⓘ	ⓘ	ⓘ
Wavelength Range	200 - 1100 nm[a]	320 - 1100 nm	340 - 1100 nm	350 - 1100 nm	350 - 1100 nm	400 - 1100 nm	400 - 1100 nm	400 - 1100 nm
Active Area	0.8 mm^2 (Ø1.0 mm)	1.21 mm^2 (1.1 mm x 1.1 mm)	100 mm^2 (10 mm x 10 mm)	13 mm^2 (3.6 mm x 3.6 mm)	100 mm^2 (10 mm x 10 mm)	0.018 mm^2 (Ø150 µm)	0.049 mm^2 (Ø0.25 mm)	0.049 mm^2 (Ø0.25 mm)
Rise/Fall Time[b]	1 ns / 1 ns @ 830 nm, 10 V	400 ns[c,d] @ 650 nm, 0 V	150 ns / 150 ns[d] @ 5 V	10 ns / 10 ns[d] @ 632 nm, 20 V	65 ns / 65 ns[d] @ 632 nm, 5 V	35 ps / 200 ps @ 850 nm, 5 V	47 ps / 246 ps @ 850 nm, 5 V	47 ps / 246 ps @ 850 nm, 5 V
NEP ($W/Hz^{1/2}$)	5.0×10^{-14} @ 830 nm, 10 V	6.8×10^{-16} @ 960 nm, 0 V	1.50×10^{-14} @ 960 nm	1.2×10^{-14} @ 900 nm, 20 V	2.07×10^{-13} @ 970 nm, 5 V	8.60×10^{-15} @ 850 nm, 5 V	9.29×10^{-15} @ 850 nm, 5 V	9.29×10^{-15} @ 850 nm, 5 V
Dark Current	0.3 nA (Typ.) @ 10 V	2.0 pA (Max) @ 10 mV	200 pA @ 5 V	1.0 nA (Typ.) @ 20 V	600 nA (Max) @ 5 V	0.03 nA (Typ.) @ 5 V	35 pA (Typ.) @ 5 V	35 pA (Typ.) @ 5 V
Junction Capacitance	6 pF (Typ.) @ 10 V	140 pF (Typ.) @ 0 V	380 pF @ 5 V	24 pF (Typ.) @ 20 V	375 pF (Typ.) @ 5 V	0.65 pF (Typ.) @ 5 V	1.4 pF (Typ.) @ 5 V	1.4 pF (Typ.) @ 5 V
Package	TO-5	TO-18	Ceramic	TO-5	Ceramic	TO-46	TO-46, FC/PC Bulkhead	TO-46
Compatible Sockets	STO5S STO5P	STO46S STO46P	Not Available	STO5S STO5P	Not Available	STO46S STO46P	STO46S STO46P	STO46S STO46P
Multipacks Available	-	-	-	5 Pack (-P5) 10 Pack (-P10) 50 Pack (-P50)	-	-	-	-

a. When long-term UV light is applied, the product specifications may degrade. For example, the product's UV response may decrease and the dark current may increase. The degree to which the specifications may degrade is based upon factors such as the irradiation level, intensity, and usage time.
b. Typical Values; R_L = 50 Ω Unless Otherwise Specified
c. Measured with a 1 kΩ Resistor
d. The photodiode will be slower at NIR wavelengths.

Universal (11 Items)

Items Ship from Newton, NJ

Item		Docs	Available	Price	Qty
FDS010	Si Photodiode, 1 ns Rise Time, 200 - 1100 nm, Ø1 mm Active Area		Today	$56.56	1
FD11A	Si Photodiode, 400 ns Rise Time, 320 - 1100 nm, 1.1 mm x 1.1 mm Active Area		Today	$17.12	1
FDS10X10	Si Photodiode, 150 ns Rise Time, 340 - 1100 nm, 10 mm x 10 mm Active Area		Today	$134.73	1
FDS100	Si Photodiode, 10 ns Rise Time, 350 - 1100 nm, 3.6 mm x 3.6 mm Active Area		Today	$17.55	1
FDS100-P5	Si Photodiode, 10 ns Rise Time, 350 - 1100 nm, 3.6 mm x 3.6 mm Active Area, 5 Pack		Today	$84.87	1
FDS100-P10	Si Photodiode, 10 ns Rise Time, 350 - 1100 nm, 3.6 mm x 3.6 mm Active Area, 10 Pack		Today	$163.74	1

Item		Docs	Available	Price	Qty
FDS100-P50	Si Photodiode, 10 ns Rise Time, 350 - 1100 nm, 3.6 mm x 3.6 mm Active Area, 50 Pack		Today	$788.17	1
FDS1010	Si Photodiode, 65 ns Rise Time, 350 - 1100 nm, 10 mm x 10 mm Active Area		Today	$65.46	1
FDS015	Si Photodiode, 35 ps Rise Time, 400 - 1100 nm, Ø150 µm Active Area		Today	$63.03	1
FDS02	Si Photodiode, 47 ps Rise Time, 400 - 1100 nm, Ø0.25 mm Active Area, FC/PC Bulkhead		Today	$98.18	1
FDS025	Si Photodiode, 47 ps Rise Time, 400 - 1100 nm, Ø0.25 mm Active Area		Today	$40.36	1

Black Si Photodiodes - 240 to 1170 nm



- Higher Responsivity Across Wavelength Range Compared to Standard Si Photodiodes
- Mounted in a Hermetically Sealed Package with a Schott UV-Glass Window

Table G2.1 Specifications

Item #[a]	Info	Wavelength Range	Active Area	Package	Rise/Fall Time[b]	NEP ($W/Hz^{1/2}$)	Dark Current	Junction Capacitance	Compatible Sockets
FDBS11		240 - 1170 nm	1.0 mm^2 (1.0 mm x 1.0 mm)	TO-46	15 ns / 19 ns @ 650 nm, 10 V	5.8×10^{-15} (Typ.) @ 1010 nm, 10 mV	250 pA (Max) @ 10 V	4 pF (Typ.) @ 10 V	STO46S STO46P
FDBS22			4.0 mm^2 (2.0 mm x 2.0 mm)		25 ns / 29 ns @ 650 nm, 10 V	7.1×10^{-15} (Typ.) @ 1010 nm, 10 mV	1 nA (Max) @ 10 V	13 pF (Typ.) @ 10 V	
FDBS25			25 mm^2 (5.0 mm x 5.0 mm)	TO-8	90 ns / 90 ns @ 650 nm, 10 V	9.2×10^{-15} (Typ.) @ 1010 nm, 10 mV	2 nA (Max) @ 10 V	55 pF (Typ.) @ 10 V	STO8S STO8P

a. All measurements are performed at 25 °C ambient temperature.
b. Typical Values; $R_L = 50\ \Omega$

Universal (3 Items) Items Ship from Newton, NJ

Item		Docs	Available	Price	Qty
FDBS22	Black Si Photodiode, 25 ns Rise Time, 240 - 1170 nm, 2.0 mm x 2.0 mm Active Area		Today	$315.65	1
FDBS11	Black Si Photodiode, 15 ns Rise Time, 240 - 1170 nm, 1.0 mm x 1.0 mm Active Area		Today	$321.00	1
FDBS25	Black Si Photodiode, 90 ns Rise Time, 240 - 1170 nm, 5.0 mm x 5.0 mm Active Area		Today	$94.16	1

Dual Band Si/InGaAs Photodiode - 400 to 1800 nm



- Dual Detector Chip Design - Si Over InGaAs - Provides Wide Detector Range
- 4-Pin TO-5 Package
- Large Active Area

Table G3.1 Specifications

Item #	Info	Wavelength Range	Active Area	Package	Rise/Fall Time[a]	NEP ($W/Hz^{1/2}$)	Dark Current	Junction Capacitance	Compatible Sockets
DSD2	i	400 - 1100 nm (Si) 1000 - 1800 nm (InGaAs)	5.07 mm^2 (Ø2.54 mm, Si) 1.77 mm^2 (Ø1.50 mm, InGaAs)	TO-5	4.0 µs (Both Layers) @ 0 V	1.9×10^{-14} (Si) 2.1×10^{-13} (InGaAs)	1 nA @ 1 V (Si) 0.5 nA @ 1 V (InGaAs)	450 pF @ 0 V (Si) 300 pF @ 0 V (InGaAs)	Not Available

a. Typical Values; R_L = 50 Ω Unless Otherwise Specified

Universal (1 Item) — Items Ship from Newton, NJ

Item		Docs	Available	Price	Qty
DSD2	Dual Band Si/InGaAs Detector, 4 µs Rise Time, 400 - 1800 nm, Ø2.54/Ø1.5 mm		Today	$710.53	1

Ge Photodiodes - 800 to 1800 nm

Table G4.1 Specifications

Click Image for Details				
Item #	FDG03	FDG05[a]	FDG50	FDG10X10
Key Feature	Large Active Area in a TO-5 Can	High Speed on a Ceramic Substrate	Large Active Area in a TO-8 Can	Largest Active Area
Info	ⓘ	ⓘ	ⓘ	ⓘ
Wavelength Range	800 - 1800 nm	800 - 1800 nm	800 - 1800 nm	800 - 1800 nm
Active Area	7.1 mm^2 (Ø3 mm)	19.6 mm^2 (Ø5 mm)	19.6 mm^2 (Ø5 mm)	100 mm^2 (10 mm x 10 mm)
Rise/Fall Time[b]	600 ns / 600 ns @ 3 V	220 ns / 220 ns @ 3 V	220 ns / 220 ns (Typ.) @ 10 V	10 µs (Typ.) @ 1 V
NEP	2.6 x 10^{-12} W/$Hz^{1/2}$ @ 1550 nm	4.0 x 10^{-12} W/$Hz^{1/2}$ @ 1550 nm	4.0 x 10^{-12} W/$Hz^{1/2}$ @ 1550 nm	4.0 x 10^{-12} W/$Hz^{1/2}$ @ 1550 nm[c]
Dark Current	4.0 µA (Max) @ 1 V	40 µA (Max) @ 3 V	60 µA (Max) @ 5 V	50 µA (Max) @ 0.3 V
Junction Capacitance	6 nF (Typ.) @ 1 V 4.5 nF (Typ.) @ 3 V	3000 pF (Typ.) @ 3 V	1800 pF (Max) @ 5 V 16000 pF (Max) @ 0 V	80 nF (Typ.) @ 1 V 135 nF (Typ.) @ 0 V
Shunt Resistance	25 kΩ (Min)	-	4 kΩ (Typ.)	2 kΩ (Min)
Package	TO-5	Ceramic	TO-8	Ceramic
Compatible Sockets	STO5S STO5P	Not Available	STO8S STO8P	Not Available

a. Please note that the wire leads on the FDG05 and FDG10X10 are attached to the sensor using a conductive epoxy, as soldering them on would damage the sensor. This results in a fragile bond. Care should be taken while handing this unit so that the wire leads are not broken.
b. Typical Values; R_L = 50 Ω Unless Otherwise Specified
c. NEP is Specified for the Photovoltaic Mode

Universal (4 Items)

Items Ship from Newton, NJ

Item		Docs	Available	Price	Qty
FDG03	Ge Photodiode, 600 ns Rise Time, 800 - 1800 nm, Ø3 mm Active Area		Today	$162.69	1
FDG05	Ge Photodiode, 220 ns Rise Time, 800 - 1800 nm, Ø5 mm Active Area		Today	$310.14	1
FDG50	Ge Photodiode, 220 ns Rise Time, 800 - 1800 nm, Ø5 mm Active Area		Today	$344.45	1
FDG10X10	Ge Photodiode, 10 µs Rise Time, 800 - 1800 nm, 10 mm x 10 mm Active Area			$585.69	1

InGaAs Photodiodes - 800 to 2600 nm

Table G5.1 Specifications

Click Image for Details								
Item #	FGA01	FGA01FC	FGA015	FDGA05	FGA21	FGA10	FD05D	FD10D
Key Feature	High Speed and Low Capacitance in a TO-46 Can with a Ball Lens	High Speed and Low Capacitance in a Direct Fiber-Coupled FC/PC Package	High Speed and Low Capacitance	High Speed, High Responsivity, and Low Capacitance	Large Active Area and High Speed	High Speed and Low Dark Current	Long Wavelength Range	Long Wavelength Range and Large Active Area
Info	ⓘ	ⓘ	ⓘ	ⓘ	ⓘ	ⓘ	ⓘ	ⓘ
Wavelength Range	800 - 1700 nm	800 - 1700 nm	800 - 1700 nm	800 - 1700 nm	800 - 1700 nm	900 - 1700 nm	900 - 2600 nm	900 - 2600 nm
Active Area	0.01 mm^2 (Ø120 µm)	0.01 mm^2 (Ø120 µm)	0.018 mm^2 (Ø150 µm)	0.196 mm^2 (Ø0.5 mm)	3.1 mm^2 (Ø2 mm)	0.79 mm^2 (Ø1 mm)	0.20 mm^2 (Ø0.5 mm)	0.79 mm^2 (Ø1.0 mm)
Rise/Fall Time[a]	300 ps / 300 ps @ 5 V	300 ps / 300 ps @ 5 V	300 ps / 300 ps @ 1550 nm, 5 V	2.5 ns / 2.5 ns @ 5 V	25 ns / 25 ns @ 3 V	10 ns / 10 ns @ 5 V	17 ns / 17 ns @ 0 V	25 ns / 25 ns @ 0 V
NEP ($W/Hz^{1/2}$)	4.5×10^{-15} @ 1500 nm	4.5×10^{-15} @ 1500 nm	1.3×10^{-14} @ 1550 nm	2.0×10^{-14} @ 1550 nm	6.0×10^{-14} @ 1550 nm	2.5×10^{-14} @ 1550 nm, 5 V	5.0×10^{-13} @ 2300 nm	1.0×10^{-12} @ 2300 nm
Dark Current	0.05 nA (Typ.) @ 5 V	0.05 nA (Typ.) @ 5 V	0.5 nA (Typ.) @ 5 V	6 nA (Typ.) @ 5 V	50 nA (Typ.) @ 1 V	1.1 nA (Typ.) @ 5 V	1 µA (Typ.) @ 0.5 V	3 µA (Typ.) @ 0.5 V
Junction Capacitance	2.0 pF (Typ.) @ 5 V	2.0 pF (Typ.) @ 5 V	1.5 pF (Typ.) @ 5 V	10 pF (Typ.) @ 5 V	100 pF (Typ.) @ 3 V	80 pF (Typ.) @ 5 V	140 pF (Typ.) @ 0 V	500 pF (Typ.) @ 0 V
Package	TO-46	TO-46, FC/PC Bulkhead	TO-18	TO-46	TO-5	TO-5	TO-18	TO-18
Compatible Sockets	STO46S STO46P	STO46S STO46P	STO46S STO46P	STO46S STO46P	STO5S STO5P	STO5S STO5P	STO46S STO46P	STO46S STO46P

a. Typical Values; R_L = 50 Ω Unless Otherwise Specified

Universal (8 Items)

Items Ship from Newton, NJ

Item		Docs	Available	Price	Qty
FGA01	InGaAs Photodiode, 300 ps Rise Time, 800-1700 nm, Ø0.12 mm Active Area		Today	$73.72	1
FGA01FC	InGaAs Photodiode, 300 ps Rise Time, 800-1700 nm, Ø0.12 mm Active Area, FC/PC Bulkhead		Today	$186.84	1
FGA015	InGaAs Photodiode, 300 ps Rise Time, 800-1700 nm, Ø150 µm Active Area			$68.76	1
FDGA05	InGaAs Photodiode, 2.5 ns Rise Time, 800-1700 nm, Ø0.5 mm Active Area			$174.14	1
FGA21	InGaAs Photodiode, 25 ns Rise Time, 800-1700 nm, Ø2 mm Active Area		Today	$283.44	1
FGA10	InGaAs Photodiode, 10 ns Rise Time, 900-1700 nm, Ø1 mm Active Area		Today	$194.81	1
FD05D	InGaAs Photodiode, 17 ns Rise Time, 900-2600 nm, Ø0.5 mm Active Area		Today	$149.98	1
FD10D	InGaAs Photodiode, 25 ns Rise Time, 900-2600 nm, Ø1.0 mm Active Area		Today	$265.66	1

TrustedSite CERTIFIED SECURE

FDG10X10

Ge Photodiode, 10 µs Rise Time, 800 - 1800 nm, 10 mm x 10 mm Active Area

Specs | Responsivity | Dark Current | Pin Diagram

Specifications[a]	
Sensor Material	Ge
Wavelength Range	800 - 1800 nm
Peak Wavelength	1550 nm (Typ.)
Responsivity[b]	0.95 A/W (Typ.)
Active Area	100 mm^2 (10 mm x 10 mm)
Rise/Fall Time (R_L = 50 Ohms, 1 V)	10 µs (Typ.)
NEP (1550 nm)[c]	4.0×10^{-12} $W/Hz^{1/2}$ (Typ.)
Dark Current (0.3 V)	50 µA (Max)
Capacitance	80 nF (Typ.) @ 1 V 135 nF (Typ.) @ 0 V
Shunt Resistance	2000 Ohm (Typ.)
Package	Ceramic

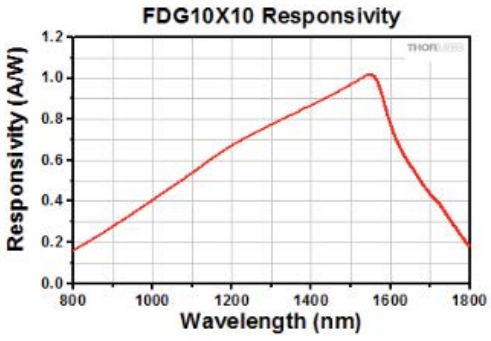
Max Ratings	
Max Bias (Reverse) Voltage	1 V
Reverse Current	10 mA
Operating Temperature	-40 to 85 °C
Storage Temperature	-40 to 125 °C

a. Unless otherwise noted, all measurements are performed at 25 °C ambient temperature.
b. Responsivity Specified at the Peak Wavelength
c. NEP is Specified for the Photovoltaic Mode

FDG10X10

Ge Photodiode, 10 µs Rise Time, 800 - 1800 nm, 10 mm x 10 mm Active Area

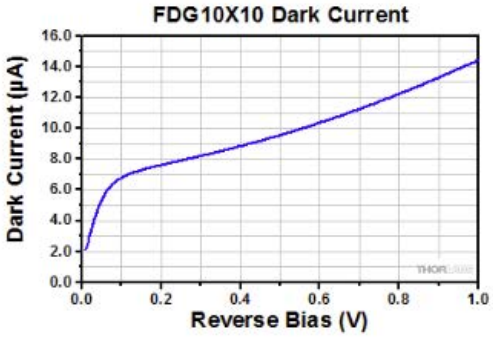
Specs | Responsivity | Dark Current | Pin Diagram



Click Here for Raw Data

FDG10X10
Ge Photodiode, 10 µs Rise Time, 800 - 1800 nm, 10 mm x 10 mm Active Area

Specs | Responsivity | Dark Current | Pin Diagram



This is a sample curve of the dark current. Actual performance will vary from photodiode to photodiode. Do not exceed the 1 V maximum reverse bias voltage.

FDG10X10
Ge Photodiode, 10 µs Rise Time, 800 - 1800 nm, 10 mm x 10 mm Active Area

Specs | Responsivity | Dark Current | Pin Diagram

